Distance Dependence of Electron-Transfer Reactions in Organized Systems: The Role of Superexchange and Non-Condon Effects in Photosynthetic Reaction Centers

Stefan Franzen,* Robert F. Goldstein,† and Steven G. Boxer

Department of Chemistry, Stanford University, Stanford, California 94305-5080

Received: August 6, 1992; In Final Form: January 8, 1993

Extremely long distance electron transfer is observed in some photosynthetic reaction centers. For several charge recombination reactions, the rate appears to fall off much more slowly with distance than expected from simple models. A general model is proposed for sequential electron-transfer reactions, which often occur in biological systems, in which each ion pair in the forward direction acts as the mediating state for recombination of the next ion-pair in the sequence. Inclusion of these mediating states in a conventional superexchange formalism improves the agreement between theory and experiment, but the results are far from satisfactory. Because the energy gap between the reactant and mediating state is small for some of these reactions, the next level of analysis is to explicitly consider non-Condon effects by using a two-state model. This gives a substantial improvement in the agreement between theory and experiment. We conclude that (1) superexchange coupling is likely quite significant for the long-distance charge recombination reactions in bacterial RCs at cryogenic temperature, (2) the coupling provided by low-lying intermediates states is often accompanied by significant non-Condon effects within a two-state model, and (3) both of these effects can significantly alter the dependence of the rate on distance. Implications of these results for the initial ultrafast charge separation step are discussed.

1. Introduction

Long-distance electron transfer between redox centers that are not covalently connected is widespread in biological systems. One difficulty in analyzing the rate constants for these reactions from first principles is that the overlap of the wave functions on the donor and acceptor is poorly known and is sensitive to the nature of the intervening matter. An essential feature of biological systems is that the matrix surrounding the reactive elements, including the matrix between these components, is organized. Consequently, some of the same issues arise for electron transfer in nonbiological, organized systems such as molecular crystals, Langmuir–Blodgett films, covalently connected donors and acceptors, and fabricated microstructures.

The photosynthetic reaction center (RC) is one of the best characterized organized electron-transfer systems. This membrane protein contains as many as eight redox centers in fixed locations. The three-dimensional structures of RCs from several species are known to atomic resolution,[1-3] and the kinetics of electron transfer for forward charge separation (CS) and reverse charge recombination (CR) reactions have been studied over a wide range of timescales (fs to s) and conditions (temperature, pH, ionic strength, pressure).[4-9] The RC is a self-contained electron-transport chain with the redox components arranged in a roughly linear fashion as shown in Figure 1 for *Rps. viridis*. Both electrons and holes move apart in the forward reactions, with the ultimate charge separation distance being about 70 Å.

The medium between any two redox centers in the RC consists of the peptide backbone, amino acid side chains, and other redox components. Redox components will always be present for systems involving a series of electron-transfer reactions. In such cases it is reasonable to propose a simple and general model in which each redox intermediate in a forward reaction serves to mediate the recombination reaction for the next charge-separated species. In a generic reaction scheme, if D is a donor and A_1, A_2, etc. are a series of acceptors, then the forward reactions are

$$DA_1A_2 \rightarrow D^+A_1^-A_2 \rightarrow D^+A_1A_2^- \qquad (1)$$

and the long-distance $D^+A_1A_2^- \rightarrow DA_1A_2$ reverse recombination reaction may involve activated formation of $D^+A_1^-A_2$ or $DA_1^+A_2^-$ at a sufficiently high temperature. Both $D^+A_1^-A_2$ and $DA_1^+A_2^-$ may also function as virtual intermediates coupling $D^+A_1A_2^-$ and DA_1A_2 at low temperature. This general principle was introduced in earlier work on long-distance CR in photosynthetic RCs where it was demonstrated that it is quantitatively consistent with available kinetic data for $P^+Q_A^-$ recombination discussed below.[10]

Although virtual coupling (superexchange) will be especially important for a system consisting of a series of redox carriers whose orbital energies are not much different, a similar mechanism can be invoked to explain through-bond coupling in protein systems or small molecules.[11,12] Superexchange via hole transfer ($DA_1^+A_2^-$) may be the dominant mechanism when the orbital energies of filled levels (valence band) of the medium are not far from those of the redox carriers. Conversely, if the LUMO of the bridge (conduction band) is closer in energy to the donor and acceptor energies, electron transfer ($D^+A_1^-A_2$) dominates the coupling. Coupling through protein and saturated spacer bridge states has been treated in detail by Onuchic and Beratan.[13-15] They concluded that the Condon approximation breaks down when the energy gap between the transferring electron and a bridge state is small or when the distance between donor and acceptor is large.[17] In the latter case, at long distances (>15 Å) there is an increased tunneling probability (i.e., the effective barrier to electron tunneling is reduced) due to electron tunneling from relatively high energy levels in the donor. Clearly the probability of such electron transfer is quite low, and that is why these effects are only considered at quite long distances. In such a case, the wave functions used to describe the reduced tunneling barrier do not obey the Born–Oppenheimer approximation.[16,17] Although these considerations apply to electronic coupling through any bridge, a significant superexchange contribution may obviate the need to consider such a low probability event by effectively lowering the tunneling barrier by means of available energy levels in the bridge.

Redox active components can act as a bridge in the same sense as residues in the protein or covalent connectors, but their redox potentials may be much closer to the redox potential of the reacting species. The proximity of the bridge energy levels serves to reduce the electron tunneling barrier. In this paper, we shall show that

† Computer Center m/c 135 and Department of Chemistry, University of Illinois at Chicago, Chicago, IL 60680.

0022-3654/93/2097-3040$04.00/0

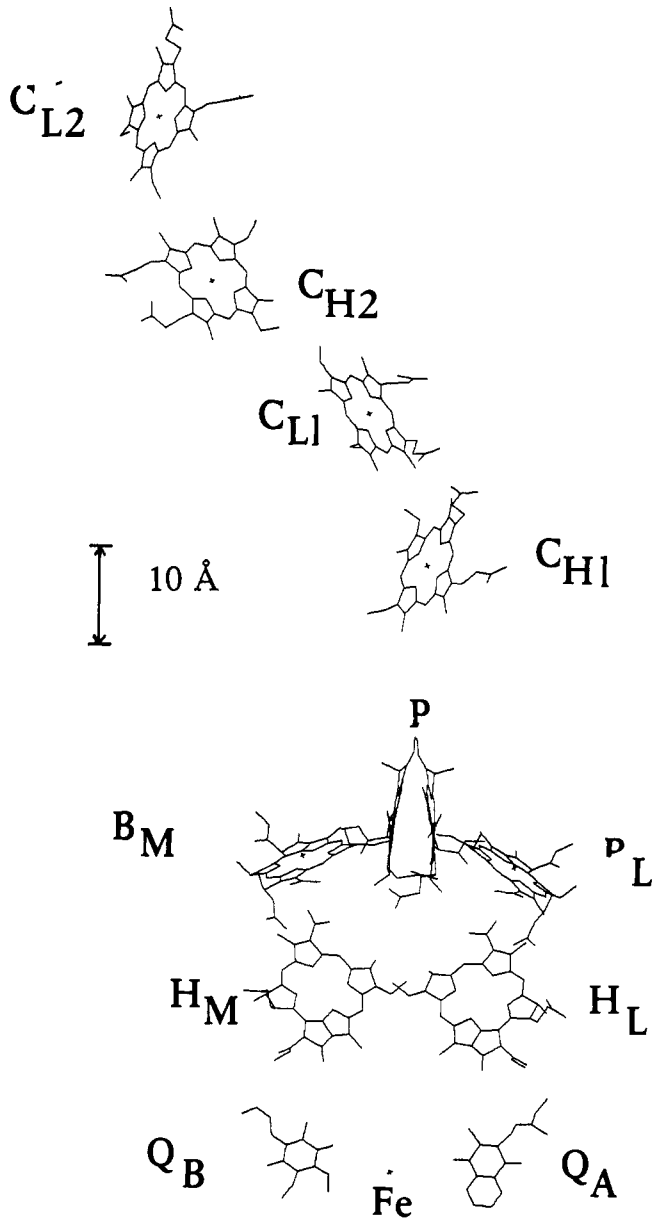

Figure 1. Schematic diagram of the reactive components in the *Rps. viridis* RC.[1] P is the bacteriochlorophyll dimer whose excited singlet state is the initial donor; H_L is a monomeric bacteriopheophytin that accepts an electron from ^1P; Q_A is menaquinone. The four hemes at the top are embedded in the cytochrome subunit, which is bound to the RC protein. C_{H1} and C_{H2} are the high potential hemes; C_{L1} and C_{L2} are the low potential hemes.

the electronic coupling depends strongly on the nuclear coordinates when the bridge state potential energy surface is close to that of the transition state (the crossing of reactant and product surfaces). Thus, superexchange through a specific redox center can give rise to a breakdown of the Condon approximation within a two-state model at any electron tunneling distance, which reduces the effective electron tunneling barrier. This effect on the tunneling barrier can be included in the coupling pathways through the protein[13-15] and contributes to an enhanced probability of long-distance electron tunneling.[17] Effective tunneling barriers have been addressed by Kuznetsov and Ulstrup in a discussion of the free-energy dependence of the electronic factor due to the polarization of the medium.[18-21] The breakdown of the Condon approximation has also been widely discussed in the context of radiationless processes in simple aromatic molecules.[22-30]

The inclusion of a bridge state with both electronic and vibrational quantum numbers formally requires a three-state calculation, and analytical solutions have not yet proven useful for the practical calculation of rate constants.[31] The role of the nuclear factor in a three-state problem has been discussed by Lin,[32] and an expansion of the three-state correlation function has been worked out by Joseph and Bialek.[33] Reimers and Hush[34,35] showed that two-state models are no longer valid when the intermediate state (bridge) is in resonance with the donor–acceptor crossing point. Using their criteria for resonance ($\Delta U \leq V_{13}$, see below), all of the case studies in this paper are nonresonant. The important conceptual connection with resonance Raman spectroscopy[32,36] will be discussed further below.

In photosynthetic systems, superexchange has most often been considered at a qualitative level, the most important factor being the dependence of the electronic coupling on the energy difference between the mediating state and the transition state.[36-41] What is seldom discussed is that, as a consequence, the electronic coupling becomes explicitly dependent on nuclear coordinates, so the usual separation of electronic and nuclear degrees of freedom is not valid. Furthermore, it is often assumed that the value of the superexchange matrix element should be calculated at the crossing point (i.e., transition state of the electron-transfer reaction). However, at low temperature when nuclear tunneling dominates the rate, the probability of reaching the transition-state configuration may be very small for any finite barrier. Thus, application of a superexchange matrix element calculated only at the nuclear coordinate of the transition state is not necessarily valid over a range of temperature. An estimate of the electronic factor that is obtained by thermally averaging the nuclear-coordinate-dependent electronic matrix element over the vibrational levels in the reactant manifold overestimates the rate constant because it completely ignores the Franck–Condon factor. To correctly calculate a rate constant, the dynamics of nuclear motion must be included in a calculation of the nuclear overlap factors weighted by the electronic factor as a function of the nuclear coordinate.

In the following, the standard model is extended to include this nuclear coordinate dependence by considering it as a non-Condon effect within the framework of a two-state model. Details of the computational methodology are given elsewhere.[42] Although clearly an approximate method, we specifically focus on how the inclusion of such effects can alter the calculated distance dependence of electron transfer, and these results are compared with data obtained for the *Rps. viridis* RC. In section 2 the unusual distance dependence of electron transfer in RCs is discussed. Section 3 discusses the issues that arise in calculations of superexchange matrix elements, some approximate models, and dephasing. The results of model calculations on the CR reactions in the RC are discussed in section 4, along with some discussion of the CS steps.

2. Properties of the Reaction Center and the Challenge

2.1. Temperature and Distance Dependence of Charge Recombination in RCs. The redox components of interest in this paper are illustrated in Figure 1. They include cytochromes c556 (C_{H2}), c559 (C_{H1}), and c553 (C_{L1});[4,43-47] the primary electron donor (a dimeric pair of bacteriochlorophylls denoted P whose first singlet excited state, ^1P, initiates the electron-transfer reactions); a monomeric bacteriochlorophyll (B_L); monomeric bacteriopheophytin (H_L); and a quinone (Q_A). The slow, long-distance recombination reactions of $P^+Q_A^-$, $C_{H1}^+Q_A^-$, and $C_{H2}^+Q_A^-$ in *Rps. viridis* have been investigated by Wraight[4] and Shuvalov and their co-workers[5] as a function of temperature and pH.[48] The reaction scheme has been characterized by both transient absorption and EPR.[4,5,45-47] The kinetics and best estimates for the energetics are illustrated in Figure 2. The edge-to-edge distance between P and Q_A is 22.5 Å,[1] and the $P^+Q_A^- \rightarrow PQ_A$ CR reaction has a rate constant of 100 s^{-1} at 150 K.[7] At the same temperature, the $C_{H1}^+Q_A^-$ CR reaction has a rate constant of ca. 2 s^{-1} over a distance of ~43 Å, and the $C_{H2}^+Q_A^-$

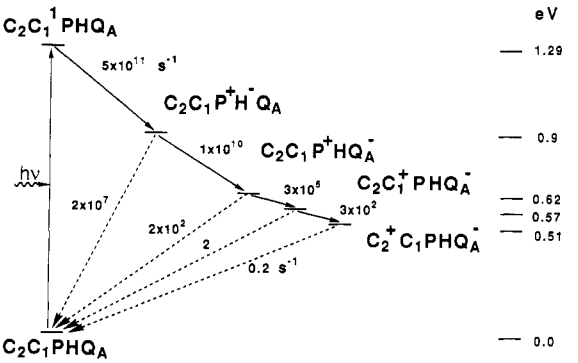

Figure 2. Reaction scheme, kinetics, and energetics for charge separation and recombination reactions in *Rps. viridis* RCs at medium redox potential (E_m > 300 mV) and 150 K.[4] C_1 and C_2 are cytochromes C_{H1} and C_{H2} shown in Figure 1.

recombination reaction has a recombination rate of ca. 0.02–0.2 s^{-1} over an edge-to-edge distance of ~68 Å.[4,5,48] The $P^+Q_A^-$, $C_{H1}{}^+Q_A^-$, and $C_{H2}{}^+Q_A^-$ CR reactions have similar temperature dependences consisting of an activated region above 240 K and an activationless region below 240 K. The relative rate constants of the CR reactions can be explained at room temperature by postulating equilibria among the three charge-separated states $P^+Q_A^-$, $C_{H1}{}^+Q_A^-$, and $C_{H2}{}^+Q_A^-$. However, as pointed out by Gao et al.,[4] such equilibria cannot account for the rate constants in the temperature-independent regime below 240 K. The much slower $C_{L1}{}^+Q_A^-$ CR is consistent with an equilibrium between $C_{L1}{}^+Q_A^-$ and $C_{H1}{}^+Q_A^-$ of the same type proposed for P, C_{H1}, and C_{H2}[4] with a larger energy gap of 2300 cm^{-1} between $C_{L1}{}^+Q_A^-$ and $C_{H1}{}^+Q_A^-$.[49] Below 200 K and at E_m < 0 mV the formation of $C_{L1}{}^+Q_A^-$ is irreversible.[5]

2.2. Failure of Exponential Distance Dependence. The rates of electron-transfer reactions are thought to fall off exponentially with distance due to the exponential falloff of the radial part of the wave functions of the initial and final states.[50-52] In the Condon approximation the rate constant is decomposed into two parts, an electronic factor ($[2\pi/\hbar]V^2$) and a nuclear or Franck–Condon factor (FC). The distance dependence is thought to reside primarily in V with $V^2 = V_0^2 \exp[-\alpha R]$ or $V = V_0 \exp[-(\alpha/2)R]$, where R is the edge-to-edge distance[53] and $V_0 \simeq 100$ cm^{-1}, giving a maximal rate constant $k_0 \simeq 10^{13}$ s^{-1} when $R = 0$, on the order of a typical low-frequency vibration. The distance dependence of the rate constant is

$$k = k_0 \exp[-\alpha R] \qquad (2)$$

In many early treatments of charge transfer as a tunneling event the exponential factor α (Gamow factor) was related to the barrier height B in units of electronvolts by $\alpha = (2mB)^{1/2}/\hbar$ (m is the mass of the particle and $\hbar$ is Planck's constant).[54-56] Studies of model systems indicate that α can be as small as 1.0 for through-bond coupling and as high as 3.4 for through-space coupling.[17,57,58] Even sophisticated treatments that include medium effects find that the decrease in coupling with distance is typically exponential, although the exponent is medium dependent.[15,18,30,34,54,72] Most recent work uses the exponent as a benchmark to describe the medium as predominantly through-bond or through-space or some combination thereof.

Taking a limiting lower value of $\alpha = 1.0$ $Å^{-1}$ for the exponential distance dependence in proteins, the rate constant for $C_{H1}{}^+Q_A^-$ recombination should be on the order of 10^{-6} s^{-1}, and the rate constant for $C_{H2}{}^+Q_A^-$ recombination should be on the order of 10^{-17} s^{-1}! Compared to the experimental recombination rate constants of ca. 2 s^{-1} for $C_{H1}{}^+Q_A^-$ and 0.02–0.2 s^{-1} for $C_{H2}{}^+Q_A^-$, even the through-bond value of $\alpha = 1.0$ for the exponential falloff leaves an enormous discrepancy, as highlighted in Figure 3. It is unlikely that the enormous discrepancy between the expected and observed rate can be attributed to the Franck–Condon factor.

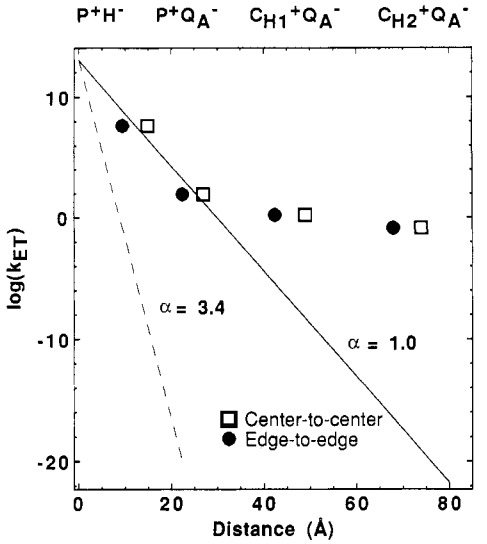

Figure 3. Distance dependence of charge recombination rates[4] in *Rps. viridis* RCs at 150 K for reactions listed at the top of the figure (center-to-center distance are the squares; edge-to-edge distances are circles). The errors in the experimental rate constants are smaller than the size of the symbols. Distances are taken from X-ray crystal structure.[1] The lines give $k_0 \exp[-\alpha R]$, where k_0 is the maximal rate constant (see text), R is the edge-to-edge distance, and α is 3.4 (- - -) and 1.0 (—).

TABLE I: Observed Charge Separation Rate Constants in *Rps. viridis* Reaction Centers at 298 K Compared with Rate Constants Calculated by Using an Exponential Distance Dependence[a]

reaction	k_{obs},[b] s^{-1}	R,[c] Å	$k_0 \exp[-\alpha R]$	V, cm^{-1}
$^1PH \rightarrow P^+H^-$	4×10^{11}	9.5	6.7×10^8	20.0
$P^+H^- \rightarrow P^+Q_A^-$	5×10^9	9.5	4.7×10^8	3.7[d]
$P^+Q_A^- \rightarrow C_{H1}{}^+Q_A^-$	3.7×10^6	10.0	8.7×10^7	0.2[e]
$P^+Q_A^- \rightarrow C_{L1}{}^+Q_A^-$[f]	6.9×10^6	16.5	5.0×10^5	0.2[e]
$C_{H1}{}^+Q_A^- \rightarrow C_{H2}{}^+Q_A^-$	2.8×10^5	21.5	5.8×10^3	0.07[e]

[a] Equation 6 and $V^2 \propto V_0^2 \exp[-\alpha R]$ with $V_0 = 100$ cm^{-1}, $\alpha = 1.0$ $Å^{-1}$. FC estimated by assuming that the reaction is activationless (FC = $1/[4\pi\lambda k_B T]^{1/2}$). V is a lower bound value for the cytochrome C_{H1} and C_{H2} oxidation reactions (see Appendix). [b] References 4, 5, and 9. [c] Edge-to-edge distances. [d] Same as in ref 113. [e] Estimates based on assumptions stated in the Appendix. [f] Reaction occurs when E_m < 100 mV.

Below 240 K all of the recombination reactions are essentially temperature independent (except $P^+H_L^-$ CR), which can be interpreted as meaning that all of the reactions are nearly activationless at low temperature.[59] Confronted with these remarkable observations, Wraight and co-workers[4] suggested that superexchange may be important in modifying the distance dependence. In the following discussion we develop a model to explore the quantitative consequences of this suggestion.

2.3. Temperature and Distance Dependence of the Charge Separation Reactions. Many of the same issues arise in attempts to explain the extremely rapid primary CS reaction rate constant, $^1P \rightarrow P^+H_L^-$. It has been suggested that superexchange via an intermediate such as $P^+B_L^-$ facilitates this primary step.[37-42] In contrast to the recombination reactions discussed above where some experimental information is available on the energy of the mediating state, the energy of the $P^+B_L^-$ state is not known; however, it is likely to be sufficiently close to the energy of ^1P that this is a viable mechanism. If the energy gap is small enough, it may be necessary to abandon the approximation that the electronic coupling is independent of the nuclear position.

The parameters relevant to the distance dependence of all of the CS reactions in *Rps. viridis* RCs are listed in Table I, and further details are given in the Appendix. The C_{L1} oxidation reaction (at $E_m \simeq 0$ mV) is faster than the C_{H1} oxidation (at E_m > 250 mV) at room temperature, even though C_{H1} is 7.0 Å closer than C_{L1} to the donor P^+.[61-65] The rate of the C_{H2} oxidation

reaction is much more rapid than expected on the basis of the exponential distance dependence. The large coupling required for this reaction has led to the suggestion that the C_{L1} cytochrome is involved in the electronic coupling for the $C_{H1}{}^{+}Q_A{}^{-} \rightarrow C_{H2}{}^{+}Q_A{}^{-}$ charge shift reaction.[4]

3. Theory

3.1. Non-Condon Effects in Superexchange. To first order, the rate constant for a transition between reactants Ψ_- and Ψ_+ can be written as[66]

$$k = (4\pi^2/h)|\langle\Psi_-|H|\Psi_+\rangle|^2\rho \tag{3}$$

where ρ is the density of states and H is the part of the Hamiltonian that causes the transition and may contain overlap terms, adiabatic breakdown terms, etc. The reactant Ψ_- and product Ψ_+ states are usually taken to be Born–Oppenheimer states that can be written as[67]

$$\Psi(Q,q) = \psi(Q,q)\chi(Q) \tag{4}$$

where Qs are nuclear coordinates, qs are electron coordinates, ψ is the electronic part of the wave function, and χ is the nuclear part. The transition matrix element becomes

$$\langle\Psi_-|H|\Psi_+\rangle = \langle\chi_-|\langle\psi_-|H|\psi_+\rangle|\chi_+\rangle \tag{5}$$

in which integration over both the electronic and nuclear coordinates is signified by $\langle\cdots\rangle$. The Condon approximation[68] is the assumption that $\langle\psi_-|H|\psi_+\rangle$ is independent of Q, and therefore the matrix element can be factored into an electronic part and a vibrational part (Franck–Condon factor). In this approximation the rate constant for transition from reactant to product is

$$k = (4\pi^2/h)V^2\mathrm{FC} \tag{6}$$

where $V = \langle\psi_-|H|\psi_+\rangle$ and $\mathrm{FC} = |\langle\chi_-|\chi_+\rangle|^2\rho$.

If V does depend on the nuclear coordinates, then factoring is not possible. In some cases, the dynamics of those vibrational modes that affect V (promoting modes) are unimportant, and one can simply use an effective V whose magnitude is different from what might be estimated by the Condon approximation, but which still allows the Condon-like factoring of the matrix element. In other cases, however, the promoting mode dynamics are significant, and the apparent Franck-Condon factors must be modified. This implies changes to expressions for the temperature and free-energy dependence of the reaction rate. When low-lying bridge states couple the reactants and products states, V can easily have a large dependence on Q.

At very large distances, the direct coupling between Ψ_- and Ψ_+ is very small. In order to discuss the second-order coupling between the states Ψ_- and Ψ_+, we introduce the zero-order states specific to the case of CR considered here: 1 is the charge-separated state (reactant), 2 is the charge-separated intermediate state (bridge), and 3 is the neutral (product) state. The diabatic potential energy surfaces for the three states involved in superexchange coupling are

$$U_1(Q) = \sum_{i=1}^{N}\frac{\omega_i^2}{2}Q_i^2 + \Delta U_{13}$$

$$U_2(Q) = \sum_{i=1}^{N}\frac{\omega_i^2}{2}(Q_i - \gamma_i Q^{\mathrm{zp}}{}_i)^2 + \Delta U_{23}$$

$$U_3(Q) = \sum_{i=1}^{N}\frac{\omega_i^2}{2}(Q_i - \eta_i Q^{\mathrm{zp}}{}_i)^2 \tag{7}$$

where ω_i are the frequencies and Q_i are the mass-weighted nuclear coordinates for the ith mode.[69] The displacement of the intermediate state for the ith mode is γ_i, and the displacement of the final state is η_i. The root-mean-square zero-point displacement of the ith mode is $Q^{\mathrm{zp}}{}_i = 1/[2\omega_i]^{1/2}$. ΔU_{13} and ΔU_{23} are the internal energy changes between states 1,3 and 2,3, respectively. For simplicity, the potential energy surfaces are assumed to be harmonic with no frequency shifts. The displacements in the potential surfaces are shifts in the nuclear coordinate that occur in the course of the electron-transfer reaction, and the total displacement can be related to the reorganization energy for the reaction, e.g., $\lambda_{13} = \sum_i \omega_i\eta_i^2/4$. The dimensionless linear electron–phonon coupling constant S_i is related to the dimensionless displacement η_i by $S_i = \eta_i^2/4$. There is also a linear coupling constant for the intermediate state S_{Mi}, where $S_{\mathrm{Mi}} = \gamma_i^2/4$.

The wave functions for the three eigenstates 1, 2, and 3 can be diagonalized in the Ψ_-,Ψ_+ basis:

$$\Psi_+ = \Psi_3 + \frac{V_{23}}{U_2(Q) - U_3(Q) - i\Gamma_{23}}\Psi_2 \tag{8}$$

$$\Psi_- = \Psi_1 + \frac{V_{12}}{U_2(Q) - U_1(Q) - i\Gamma_{12}}\Psi_2 \tag{9}$$

where phenomenological damping constants Γ_{12} and Γ_{23} have been included to account for the energy width of the vibronic level in the intermediate state due to the electronic dephasing of 2 with respect to states 1 and 3, respectively. The magnitude of Γ_{12} or Γ_{23} in eqs 8 and 9 is the reciprocal of the T_2 lifetime of the intermediate state[70] (see section 3.5). The coefficients for the mixing of states 1 and 3 into state 2 result in a second-order term in the electronic coupling, which is used in calculating the electronic factor of the rate constant in eq 6. The electronic coupling as a function of the nuclear coordinate has the form

$$V(Q) = V_{13} + {}^1/_2\left[\frac{V_{12}V_{23}}{U_2(Q) - U_1(Q) - i\Gamma_{12}} + \frac{V_{12}V_{23}}{U_2(Q) - U_3(Q) - i\Gamma_{23}}\right] \tag{10}$$

This expression includes the direct coupling V_{13}, which is the first-order term (direct coupling between reactant and product states). Superexchange dominates when V_{13} is negligible compared to the second-order terms. Even when the electronic couplings V_{12} and V_{23} have no nuclear coordinate dependence,[71] the magnitude of the matrix element $V(Q)$ given by eq 10 depends on the position of the nuclear coordinate because the potential energy terms in the denominator depend on Q. The form of eq 10 is generally valid in the region of nuclear coordinate space where the reactant and product state are not in resonance.[31] The off-resonance terms given by eq 10 are often assumed not to contribute substantially to the overall electronic coupling compared to the resonant interaction given below.

At high enough temperature an electron-transfer reaction proceeds via the crossing point $Q^*{}_{13}$, which is the intersection of surfaces 1 and 3. The magnitude of $\Delta U_{21}(Q^*{}_{13}) = U_2(Q^*{}_{13}) - U_1(Q^*{}_{13})$ can be calculated by solving for the location of $Q^*{}_{13}$ in nuclear coordinate space. If only one mode is coupled to the electron-transfer process, the location of the crossing point can be found from the equation $U_3(Q^*{}_{13}) = U_1(Q^*{}_{13})$. For a multiphonon process the intersection $U_1(Q^*{}_{13}) = U_3(Q^*{}_{13})$ is used as a constraint, and the minimum is found by the method of LaGrange multipliers. At high temperature the superexchange electronic coupling is usually calculated by using the value of the state mixing obtained at the crossing point $Q^*{}_{13}$ (i.e., when states

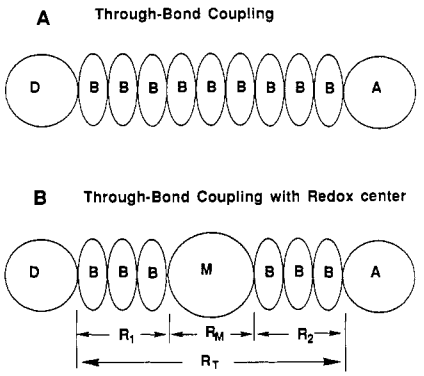

Figure 4. Schematic model for through-bond coupling (A) without and (B) with a redox center M (of diameter R_M) in the bridge. A through-bond pathway is shown with bridge atoms labeled B, which all have high-energy intermediate states. The entire group of B atoms can be considered collectively as a bridge between the donor D and acceptor A. When the electron is on molecule D, M, or A the system is in state 1, 2, or 3, respectively, for CS reactions or 3, 2, or 1, respectively, for CR reactions.

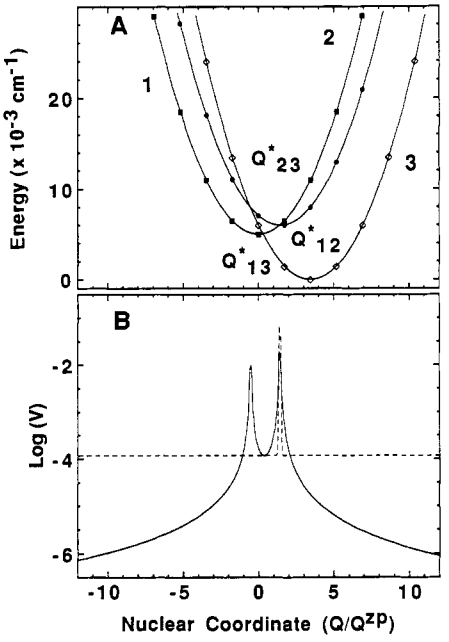

Figure 5. Potential surfaces (A) and electronic coupling (B) as a function of the nuclear coordinate: exact electronic coupling (—) and the Gaussian approximation (- - -). The equilibrium position of state 2 is 6000 cm^{-1} (0.75 eV) above the final state.

1 and 3 are in resonance)

$$V(Q^*_{13}) = V_{13} + \frac{V_{12}V_{23}}{\Delta U_{21}(Q^*_{13}) - i\Gamma_{12}} \qquad (11)$$

where there is a single dephasing rate Γ_{12} at Q^*_{13}. This electronic factor calculated at a single point in nuclear configuration space is a static superexchange approximation. Equations 10 and 11 are nonresonant and resonant electronic coupling terms, respectively, which can be derived at the simplest level by substitution of the first-order wave functions (eqs 8 and 9) into eq 6. If this is done, the magnitude of the superexchange terms in eqs 10 and 11 is twice as large as what we have given. The origin of the factor of 2 is that the first-order wave functions (eqs 8 and 9) are not orthogonal. The nonorthogonality can be corrected either by extending the wave functions to include the second-order term (thus making them orthogonal) or by correcting the resulting coupling by symmetric diagonalization. We refer the interested reader to the lucid explanation of these possibilities in ref 31.

The model employed to describe the superexchange coupling of a redox center is also valid for any type of bridge. Equation 10 can be extended to include N identical sites that occupy the space between the donor and acceptor. In the idealized case of a linear chain of identical centers in the bridge each with coupling V_B and a coupling of the bridge to the donor of V_{1B} and to the acceptor of V_{B3}, the superexchange coupling is

$$V(Q^*_{13}) = V_{1B}V_B^{N-1}V_{B3}\left[\frac{1}{\Delta U_{B1}(Q^*_{13}) - i\Gamma_B}\right]^N \qquad (12)$$

where the dephasing Γ_B between each of the coupled electronic states has been included, $\Delta U_{B1}(Q) = U_B(Q) - U_1(Q)$, and backscattering has been ignored.[13] The dephasing rate Γ_B can be ignored for bridge states that have a sufficiently large energy gap with respect to the donor/acceptor. A model for through-bond coupling of this type was first derived by McConnell.[12] Incorporation of this model of superexchange into the exponential form of the distance dependence has been considered by several groups.[15,18,72] A simplified drawing of a bridge of this type is shown in Figure 4A where molecules D and A are the donor and acceptor. The reactant state (state 1) and product state (state 3) correspond to DA and D^+A^-, respectively, for CS reactions or D^+A^- and DA, respectively, for CR reactions. In this model, state 2 is the aggregate of all bridge atoms B in Figure 4A as well as mediating molecule M in Figure 4B. If the radius of atom B in the linear chain is R_B then $\alpha = \log [V_B/2\Delta U_{B1}(Q^*_{13})]/2R_B$, and the coupling of states 1 and 3 to the bridge is obtained by viewing the entire bridge as state 2 in eq 10.

3.2. Gaussian Model Function Used in Non-Condon Calculation. The nuclear coordinate dependence of the electronic coupling can be estimated by using a Gaussian approximation to the functional dependence on nuclear coordinates in eq 10. The functional dependence of the electronic coupling in eq 10 is due to the difference in energy between states 1, 2, and 3 shown in Figure 5A. Although a Gaussian model introduces an additional level of approximation, the approximation is controlled and can be reduced with a concomitant increase in computational time, and the new functional forms retain all of the qualitative features of the "exact" $V(Q)$.

$$V(Q) = V(Q^*_{13})\{1 + A\exp[-(Q - Q_0)^2/2\sigma^2]\} \qquad (13)$$

where Q_0 is the displacement of the peak of the Gaussian from the position halfway between the reactant and product equilibrium positions, σ^2 is the variance of the Gaussian, and $A = V_{12}V_{23}/2\Gamma_{12}V(Q^*_{13})$ or $V_{12}V_{23}/2\Gamma_{23}V(Q^*_{13})$.[73,74] A simple approximate method is to equate the average coupling under the peaked area shown in Figure 5B with the average coupling of a Gaussian function. This approximation is based on the idea that the enhanced coupling strength in a region where the nuclear coordinate is near the level crossing of the bridge state with the product state contributes to the rate due to the magnitude of the coupling (height of the peaked function in Figure 5B) and the spread of nuclear coordinate where the enhanced coupling is applicable (width of the peaked function in Figure 5B). The integral of each of these functions over the region of nuclear coordinate space between the equilibrium coordinates of reactants and products was calculated analytically. The variance of the Gaussian was obtained from the calculate area $[\simeq V(Q^*_{13})\{1 + A(2\pi)^{1/2}\sigma\}]$, where A was defined above.

Once obtained, $V(Q)$ is used to calculate the rate constant by using eq 3. The evaluation of the correlation function is described elsewhere.[41] Briefly, within the Condon approximation, the electronic coupling matrix element is a constant with respect to nuclear motion and is factored out (as in eq 6). The calculation of FC is then reduced to the evaluation of the correlation function $c(\tau)$ of shifts in position of the nuclei between reactant and product states.[42] The Fourier transform of $c(\tau)$ gives the energy spectrum of the nuclear transition probability (commonly known as the rate vs free energy curve for the reaction). Because eq 13 is a function of nuclear position, it cannot be factored out of the integral

Fourier transform and acts as a weighting function, thus altering the transition probability both in overall magnitude and in terms of its frequency spectrum.

A case of strong dependence of the electronic factor on the nuclear coordinate is shown in Figure 5. The large increase in the coupling in the region of the reaction coordinate that is seen in Figure 5B is due to the crossing of potential surfaces 2 and 3 in a region of nuclear coordinate space near the equilibrium position. The average coupling near the nuclear coordinate of the intermediate state level crossing is larger than the value of the coupling at the crossing point Q^*_{13}, and this large coupling at Q^*_{23} contributes to the rate constant. There is also an increase in the coupling near the Q^*_{12} crossing point. This increase in coupling may also contribute to a non-Condon effect but is not included because it is farther from the Q^*_{13} crossing point.

3.3. Model Calculations. Returning to the generic example outlined in the introduction, the direct coupling between D and A_2 is $V_{13} = V_0 \exp[-(\alpha/2)R_T]$ where R_T is the distance between D and A_2 and α is determined by the nature of the through-bond interactions. Note the α represents the exponential factor that determines the decay of the electronic factor V^2 and therefore $\alpha/2$ is the factor that determines the decay of coupling V. If several of the atoms on the through-bond pathway are replaced by a redox center of diameter R_M as shown in Figure 4B, the coupling of the intermediate is $V_{12} = V_0 \exp[-(\alpha/2)R_1]$ and $V_{23} = V_0 \exp[-(\alpha/2)R_2]$, where $R_1 + R_2 + R_M = R_T$. From eq 11 the coupling including both direct and superexchange contributions is (ignoring Γ_{12}, see section 3.5)

$$V(Q^*_{13}) = \left[1 + \frac{V_0 \exp[(\alpha/2)R_M]}{\Delta U_{21}(Q^*_{13})}\right] V_0 \exp[-(\alpha/2)R_T] \quad (14)$$

The superexchange contribution is larger than the direct contribution to the electronic coupling when $\Delta U_{21}(Q^*_{13}) < V_0 \exp[(\alpha/2)R_M]$. Consider, for example, a donor D and acceptor A_2 that have an edge-to-edge distance R of 20 Å and $V_0 = 100$ cm^{-1}. Taking $\alpha = 1.0$ Å^{-1}, the calculated direct coupling $V_{13} \simeq 5 \times 10^{-3}$ cm^{-1}. For a redox center A_1 with $R_M = 6$ Å located 7 Å from both D and A_2, the coupling $V_{12} = V_{23} \simeq 3.0$ cm^{-1}, on the basis of the same distance dependence. In this case the superexchange coupling will be larger than the direct coupling if $\Delta U_{21}(Q^*_{13}) < 2000$ cm^{-1} (0.25 eV). In order to see when the non-Condon contribution is significant, we consider a simple system with a single promoting mode of frequency $\omega = 1000$ cm^{-1} at a temperature of 100 K. The potential surfaces shown in Figure 6 are for $S = 3$ ($\lambda = 3000$ cm^{-1} or 0.375 eV), and $\Delta G = -10\,000$ cm^{-1} (−1.25 eV), thus, this system is in the inverted region ($-\Delta G > \lambda$). In the Condon approximation the FC factor for this configuration is FC = 5×10^{-6} at 100 K, which gives rise to a recombination rate constant of $k = 125$ s^{-1}. Consider now the addition of the intermediate state with an equilibrium position $U_2(\gamma)$ and displaced from the product's equilibrium position by $S_M = 1$, where S_M is the electron–phonon coupling of the intermediate state. Table II gives ΔU_{eq}, the energy of $U_2(\gamma)$ relative to $U_1(0)$, along with the energy gap $\Delta U_{21}(Q^*_{13})$ at the crossing point. As the energy of the mediating state is varied, the position of the level crossings of the intermediate with either reactants or products are shifted as shown in Figure 6B. The resulting rate vs free energy curves are shown in Figure 7 for three configurations of potential surfaces in which the rate constant is enhanced over the direct rate constant. A significant enhancement is observed due to the non-Condon effect; typical values are given in Table II.

Figure 8A illustrates a case in the "normal" region ($-\Delta G < \lambda$), with $S = 6$ ($\lambda = 6000$ cm^{-1}, 0.75 eV) and $\Delta G = -5000$ cm^{-1} (−0.6 eV), giving FC = 10^{-3} and $k \simeq 2.5 \times 10^4$ s^{-1}. The intermediate potential surface is again taken to be at $S_M = 1$, and the resulting rates are given in Table II. Comparison of these two cases shows

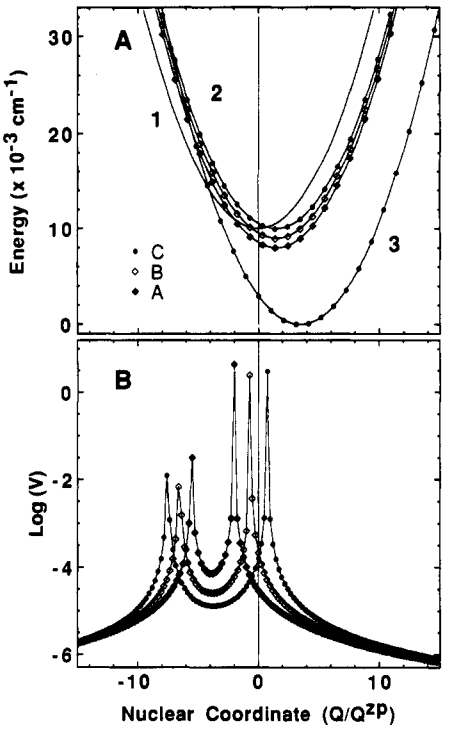

Figure 6. Potential surfaces and electronic coupling as a function of the nuclear coordinate for a single promoting mode in the inverted region ($-\Delta G > \lambda$). (A) Potential energy surfaces (eq 7) for a $\omega = 1000$ cm^{-1} and $S = 3$. The surfaces correspond to reactants (—) and products (○), with various intermediate levels: A with $\Delta G = -2000$ cm^{-1} (solid diamonds), intermediate B with $\Delta G = -1000$ cm^{-1} (hollow diamonds), and intermediate C with $\Delta G = 0$ cm^{-1} (solid circles). (B) The electronic coupling as a function of the nuclear coordinate for the potential energy surfaces shown in (A). These curves were calculated by using eq 10.

TABLE II: Model Calculation of Superexchange-Mediated Rate Constants Including the Non-Condon Effect

	normal region[a]			inverted region[b]		
$\Delta U_{21}(Q^*_{13})$, cm^{-1}	ΔU_{eq},[c] cm^{-1}	k_{SE},[d] $\times 10^{-5}$ s^{-1}	k_{NC},[d] $\times 10^{-5}$ s^{-1}	ΔU_{eq},[c] cm^{-1}	k_{SE},[d] $\times 10^{-5}$ s^{-1}	k_{NC},[d] $\times 10^{-5}$ s^{-1}
1500	0	0.87	2.2	−2000	0.042	1.6
2500	1000	0.45	0.87	−1000	0.090	8.5
3500	2000	0.37	0.45	0	0.016	7.0

[a] $\lambda = 6000$ cm^{-1}, $\Delta G = -5000$ cm^{-1}, $k_{direct} = 0.25 \times 10^5$ s^{-1}; see Figures 8 and 9. [b] $\lambda = 3000$ cm^{-1}, $\Delta G = -10\,000$ cm^{-1}, $k_{direct} = 0.0012 \times 10^5$ s^{-1}; see Figures 6 and 7. [c] $\Delta U_{eq} = U_2(\lambda) - U_1(0)$ is the equilibrium energy difference. [d] k_{SE} calculated by using superexchange within the Condon approximation (eq 11); k_{NC} calculated including the non-Condon effect.

that the largest relative change in rate constant occurs in the inverted region. This is relevant to both CR reactions with a large driving force and nearby mediating state(s)[75] and internal conversion when there are nearby states that couple to the transition.

3.4. Strategy for RC Calculations and Parameter Values. In order to apply these ideas to the RC problem, we require estimates of the electron–phonon couplings S_i and frequencies ω_i for reactant, product, and bridge states to compute the three energy surfaces $U_1(Q)$, $U_2(Q)$, and $U_3(Q)$ (eq 7), from which the dependence of V on the nuclear coordinate is obtained (eq 10). Reasonable estimates for these values for the RC are presented in the Appendix. The rate constants can then be calculated for a simple superexchange model (eq 11), and these are compared with rate constants calculated including the non-Condon effect by using the promoting mode correlation function developed in ref 42. For the purpose of calculation, a representative temperature of $T = 100$ K was used. The results are valid over the activationless region from 150 to 240 K, which was described in ref 4. All of the model calculations of the rate constants use identical parameter values.

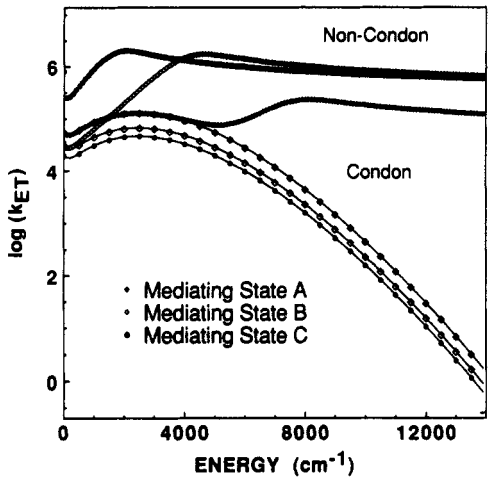

Figure 7. Rate vs free energy curves for Condon (—) and non-Condon (broken symbols) rate constant. Three pairs of curves are shown, which correspond to the three configurations of the mediating potential surfaces shown in Figure 8 (identical symbols used) in the "inverted" region: $\Delta G \simeq -1.25$ eV, $\lambda \simeq 0.375$ eV.

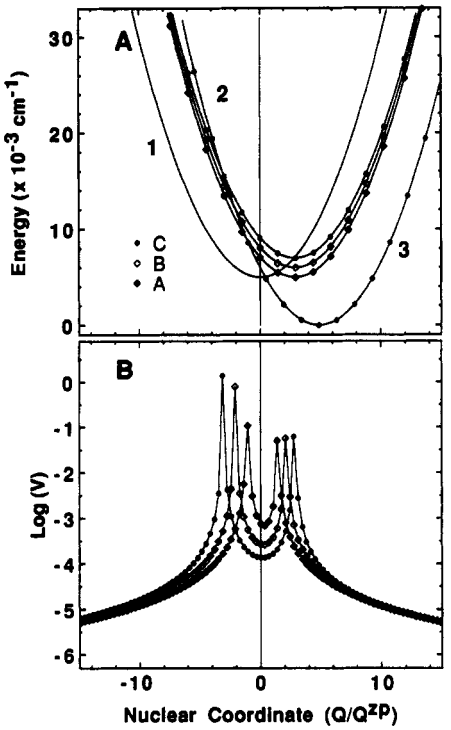

Figure 8. Potential surfaces and electronic coupling as a function of the nuclear coordinate for a single promoting mode in the normal region ($-\Delta G < \lambda$). (A) Potential energy surfaces (eq 7) for a $\omega = 1000$ cm^{-1} and $S = 6$. The surfaces correspond to reactants (—) and products (O), with various intermediate levels: A with $\Delta G = 0$ cm^{-1} (solid diamonds), intermediate B with $\Delta G = 1000$ cm^{-1} (hollow diamonds), and intermediate C with $\Delta G = +2000$ cm^{-1} (solid circles). (B) The electronic coupling as a function of the nuclear coordinate for the potential energy surfaces shown in (A). These curves were calculated by using eq 10.

In practice, it is difficult to apply the Gaussian model to more than one mode because of the simultaneous dependence of the coupling on the nuclear coordinates of all promoting modes. Even though all of the modes are in principle promoting modes according to eq 10, it is more convenient for numerical reasons to characterize the electronic coupling as a function of nuclear coordinate along a single representative mode and use that functional dependence for the calculation of the rate constant. In the calculations presented below the non-Condon effect will be calculated by using either a high-frequency ($\omega = 1600$ cm^{-1}) or low-frequency mode ($\omega = 50$ cm^{-1}) as the promoting mode. If more than two modes

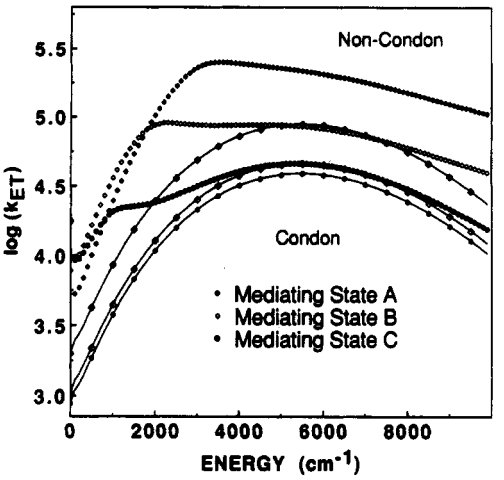

Figure 9. Rate vs free energy curves for Condon (—) and non-Condon (broken symbols) rate constant. Three pairs of curves are shown, which correspond to the three configurations of the mediating potential surfaces shown in Figure 8 (identical symbols used) in the "normal" region: $\Delta G \simeq -0.625$ eV, $\lambda \simeq 0.75$ eV.

are used, a one-dimensional slice along one of the modes only is used for the calculation of the non-Condon effect.[76]

3.5. Homogeneous and Inhomogeneous Broadening. The magnitude of Γ_{12} or Γ_{23} determines the superexchange coupling, but the magnitude of dephasing between the initial and final state Γ_{13} determines the magnitude of the FC factor in eq 6. The nuclear overlap for N modes in the low-temperature limit is given by[54]

$$FC = e^{-S}\prod_{k=1}^{N}\left[\sum_{n_k=0}^{\infty}\frac{S_k{}^n k}{n_k!}\right]\rho \tag{15a}$$

and

$$\rho = \delta(\Delta U_{13} - n_k\hbar\omega_k) \tag{15b}$$

where S_k is the electron–phonon coupling and ω_k is the frequency of the kth mode. These levels are broadened by replacing the δ function by a Lorentzian function of width Γ_{13}, which describes the density of states:

$$\rho = \frac{\Gamma_{13}}{\pi[(\Delta U_{13} - n_k\hbar\omega_k)^2 + \Gamma_{13}{}^2]} \tag{16}$$

in which $\Delta U_{13} - n_k\omega_k$ is the detuning of the reactant and product states in the crossing region. The single molecule line shape given by eqs 15 and 16 is further broadened by convolution with a Gaussian inhomogeneous linewidth, which has fwhm Γ_I. In the static limit eqs 15 and 16 give the FC factor is used with eq 11. The magnitude of Γ_{13} is not known and is sometimes assumed to be on the order of the mode frequency of the lowest frequency mode (e.g., in the coarse graining treatment of Levich[77]). When dielectric continuum theory is used to calculate the FC factor[78] the δ function in eq 15 is replaced by a Gaussian density of states:

$$\rho = \frac{1}{(4\pi\lambda_S k_B T)^{1/2}}\exp\left\{\frac{[\Delta U_{13} - n_k\hbar\omega_k + \lambda_S]^2}{4\lambda_S k_B T}\right\} \tag{17}$$

where λ_S the outer sphere (solvent) reorganization energy. The effective dephasing rate between any two states i and j is $\hbar/(4\lambda_{ij}k_BT)^{1/2}$ where λ_{ij} is the solvent reorganization energy for the transition from state i to j due to the polarization coordinate of the solvent. The fast solvent fluctuations in this limit are often considered to be a contribution to the homogeneous broadening. In this picture, the nuclei move to the crossing region Q^*_{13} where mixing with the electronic state of the product can occur for a time equal to $\hbar/(4\lambda_{13}k_BT)^{1/2}$, corresponding to an energy width of approximately $\Gamma_{13} < (4\lambda_{13}k_BT)^{1/2}$ at high temperature and Γ_{13}

$< (4\lambda_{13}\hbar\omega)^{1/2}$ at low temperature ($\hbar\omega \gg k_BT$). This limit is most often used in the effective two-state calculation of the FC factor for the vibrational overlap of states 1 and 3.[42,79] At 150 K in RCs the solvent reorganization energy is likely to be a small contribution to the total.[10] These considerations suggest that the magnitude of the levelwidth Γ_{13} in electron-transfer reactions is of the order of a typical low-frequency mode (e.g., 50 cm^{-1}). One method for experimentally estimating the magnitude of Γ_{13} for radiative transitions is comparison with values for the homogeneous linewidth from hole-burning or resonance Raman spectroscopy.

The effect of dephasing on superexchange coupling can be understood by comparing the calculation of nonradiative superexchange rates to resonance Raman cross sections. The form of the matrix element for Raman spectroscopy is the same as that in eq 10 for the nonradiative process of electron transfer.[32,36] If the (detuning) energy $\Delta U_{12} = 0$ or $\Delta U_{23} = 0$, the matrix element in eq 10 is mathematically equivalent to the calculated resonance Raman cross section. When the energies are not zero (i.e., far from level crossings of the intermediate state), the superexchange matrix element is equivalent to the preresonance or off-resonance Raman cross section. The photosynthetic system described here manifests an increase in rate for nonradiative electron transfer due to level crossings (resonances). Q^*_{12} or Q^*_{23} give rise to resonant enhancements of the tunneling rate analogous to the enhancement in scattering intensity observed when the frequency of excitation is preresonant or resonant with an electronic transition. The radiative and nonradiative cases differ in that the radiation field drives the system at the incident frequency whereas nonradiative electron transfer occurs at a frequency determined by off-diagonal coupling terms or coherences (e.g., V_{12} and V_{23}). The dynamics in the intermediate state can affect both radiative and nonradiative processes. Solvent dynamics will not affect coherences unless the time scale is on the order of the electronic coherence time (typically hundreds of femtoseconds). Motions slower than this time scale will contribute to spectral diffusion but not to the homogeneous linewidth.[80] The uncertainty principle relates the homogeneous linewidth or levelwidth to the dephasing rate $\Gamma_{12} \simeq \hbar/T_2$,[70] allowing one to obtain an estimate for Γ_{12} from spectroscopy. The comparison between the holewidth of the zero-phonon line and the electron-transfer rate of ^1P shows that $1/T_2^*$ in the RC is quite slow compared with the primary CS reaction ($T_2^* \gg 1$ ps) at $T = 1.5$ K;[81,82] thus $T_2 \simeq 2T_1 \simeq 2$ ps. Information can be obtained from the temperature dependence of resonance Raman linewidths, intensities, and excitation profiles.[83,84] The dephasing rate in the intermediate state measured by using the absolute intensity of resonance Raman scattering or linewidths of transient resonance Raman lines allows an estimate of Γ_{12}, $\Gamma_{23} < 20$ cm^{-1} for typical molecules.[85,86] The intermediate states of the CR reactions are known and the T_2^* lifetime for states such as $P^+Q_A^-$ is likely to be even longer than the value obtained for the short-lived state ^1P ($T_2^* \gg 1$ ps). In states other than ^1P, the T_1 lifetime is longer still in the zero-phonon level of the intermediate state or other levels if vibrational relaxation is on the picosecond time scale or longer.

4. Results and Discussion

4.1. Superexchange within the Condon Approximation. Tables III and IV present results for the superexchange matrix elements and rate constants, respectively, calculated at Q^*_{13} (eq 11) and by using eq 6.[36-41] The calculated rate is in reasonable agreement with experiment for $P^+Q_A^-$ CR.[10] The rate calculated for $C_{H1}{}^+Q_A^-$ recombination is a factor of 10 larger than the estimated nonmediated rate on the basis of the exponential falloff of the electronic overlap; however, it is still 5 orders of magnitude smaller than the observed rate. The rate calculated for $C_{H2}{}^+Q_A^-$ recombination reaction, taking $C_{H1}{}^+Q_A^-$ as the mediating state, is 4 orders of magnitude greater than the estimated nonmediated rate based on the exponential falloff the electronic overlap; however, it is still about 12 orders of magnitude smaller than the observed rate.

TABLE III: Calculated Superexchange Matrix Elements for Charge Recombination Reactions in *Rps. viridis* Reaction Centers Using the Condon Approximation

electronic state initial (bridge)[a]	V_{12},[b] cm^{-1}	V_{23},[b] cm^{-1}	ΔU_{21},[d] cm^{-1}	V_{SE}[c]
$P^+Q_A^-$ (P^+H^-)	3.7[d]	0.37[e]	2260.0	6.0×10^{-4}
$C_{H1}{}^+Q_A^-$ ($P^+Q_A^-$)	0.2	6.0×10^{-4}	500.0	2.4×10^{-7}
$C_{H1}{}^+Q_A^-$ ($C_{H1}{}^+PH^-$)	3.7	1.5×10^{-4}	2260.0	2.4×10^{-7}
$C_{H2}{}^+Q_A^-$ ($C_{H1}{}^+Q_A^-$)	0.07	2.4×10^{-7}	640.0	2.6×10^{-11}
$C_{H2}{}^+Q_A^-$ ($C_{H2}{}^+PH^-$)	3.7	1.7×10^{-8}	2260.0	2.6×10^{-11}

[a] The product state (state 3) is the neutral ground state PHQ_A in all cases. [b] Based on CS reactions using eq 6 (cf. Table I). [c] Calculated at the crossing point Q^*_{13} by using eq 11, assuming $\Gamma_{12} = 0$, $\Gamma_{23} = 0$, and $V_{13} = 0$. [d] Evaluated at Q^*_{13}. [e] Value consistent with analysis in refs 10 and 113.

TABLE IV: Observed Charge Recombination Rate Constants in *Rps. viridis* Compared with Rate Constants Calculated by Using an Exponential Distance Dependence and Superexchange within the Condon Approximation

recombination reactn	k_{obs},[a] s^{-1}	R,[b] Å	$k_0 \exp[-\alpha R]$[c]	k_{SE}[d]
$P^+Q_A^- \rightarrow PQ_A$	100	22.5	1.1×10^3	15.0
$C_{H1}{}^+Q_A^- \rightarrow C_{H1}Q_A$	1.85	42.5	2.3×10^{-6}	2.9×10^{-5}
$C_{H2}{}^+Q_A^- \rightarrow C_{H2}Q_A$	0.15	68	2.0×10^{-17}	3.7×10^{-13}

[a] Taken from ref 4 at 150 K. The values in ref 5 at 77 K are discussed in the text. [b] Edge-to-edge distance.[14-16] [c] From eq 6 and ($V^2 = V_0{}^2 \exp[-\alpha R]$); $V_0 = 100$ cm^{-1}, $\alpha = 1.0$ $Å^{-1}$, and FC calculated by assuming an activationless reaction (see text). [d] Calculated by using eqs 6 and 11; FC identical with value used in exponential distance dependence in adjacent column.

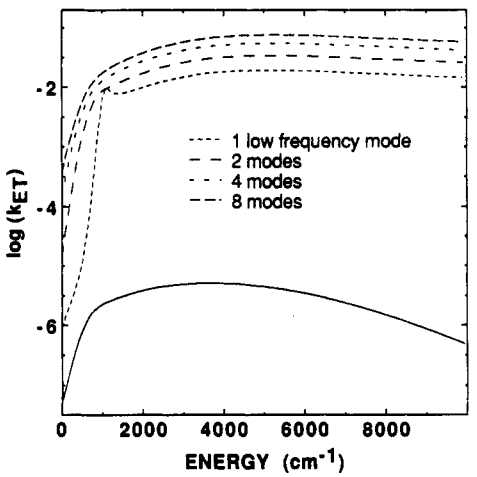

Figure 10. Non-Condon effect on the log(k) vs ΔG curve of the $C_{H1}{}^+Q_A^-$ reaction for various numbers of a 50-cm^{-1} mode (shown in the legend). The parameters used (and rate constants when $\Delta G = 3700$ cm^{-1}) are given in Table V.

4.2. Superexchange Including Non-Condon Effects for $C_{H1}{}^+Q_A^-$ Recombination. The calculated non-Condon effect on the rate constant of the reaction $C_{H1}{}^+Q_A^- \rightarrow C_{H1}Q_A$ is shown as a function of free energy in Figure 10. The calculation assumes $\lambda = 4560$ cm^{-1} is partitioned into high- and low-frequency modes with coupling constants and frequencies of $S_1 = 2.1$, $\omega_1 = 1600$ cm^{-1} and $S_2 = 24.0$, $\omega_2 = 50$ cm^{-1} (see eq A1). The magnitude of the non-Condon effect depends on the position of the maximum Q_0 of the Guassian coupling function[42] (see Table V). The magnitude of the non-Condon effect decreases as Q_0 is moved further from Q^*_{13}. When $|Q_0| > S^{1/2}$ (i.e., the maximum lies outside the nuclear trajectory for the reaction) the non-Condon effect is negligible. The small value of σ (see eq 13) means that the calculated Gaussians are so narrow as to be essentially δ functions. σ can

TABLE V: Non-Condon Effect on the $C_{H1}^+Q_A^-$ Charge Recombination Rate for Various Numbers of Low-Frequency Modes

no. of 50-cm^{-1} modes	coupling per mode	log(k_{NC})[b]	σ,[c,d] ×10^5	Q_0[c]
1	24.0	−1.8	4.0	0.63
2	12.0	−1.5	5.9	0.89
4	6.0	−1.3	8.3	1.3
6	4.0	−1.3	10.0	1.5
8	3.0	−1.2	11.0	1.8

[a] In all cases the high-frequency mode ω_1 = 1600 cm^{-1} with S_1 = 2.1. [b] Calculated by using the Gaussian model (eq 13) and Γ_{12} = 0. All rate constants are in units of s^{-1}. For these conditions log(k_{SE}) = −4.5, log(k_{obs}) ≃ 0.26. [c] σ is the standard deviation of the Gaussian (eq 13), and Q_0 is the position of the maximum in units of zero-point motion, $Q^{zp} = 1/[2\omega]^{1/2}$. [d] The amplitude factor A = 1.3 × 10^5 in all cases.

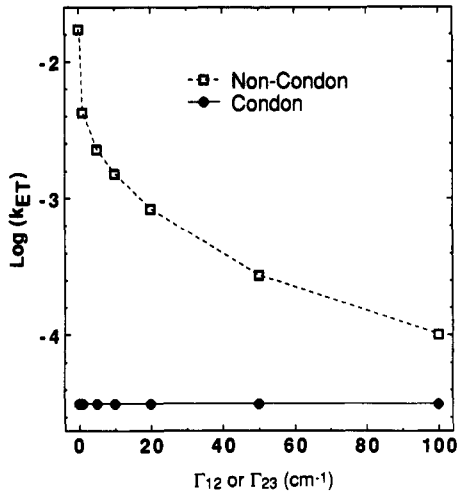

Figure 11. Non-Condon effect as a function of Γ_{12}. The squares (- - -) are a two-mode calculation including the non-Condon effect and the dark circles (—) are a two-mode calculation using the Condon approximation. The parameters used in the calculation are listed in Table V.

TABLE VI: Comparison of $C_{H1}^+Q_A^-$ Recombination Rate Constants Calculated with and without the Condon Approximation

		log(k_{NC})[c] for different mediating states			
		$P^+Q_A^-$		$C_{H1}^+H^-$	
$\lambda/\Delta G$[a]	log(k_{SE})[b]	ω_1	ω_2	ω_1	ω_2
1.26	−4.5	−3.7	−1.3	−3.3	−4.5
1.52	−4.4	−3.8	−4.4	−3.4	−0.8
1.70	−4.3	−3.8	−4.3	−3.4	−0.1
1.96	−3.9	−3.8	−3.9	−3.5	−3.8

[a] ΔG = −3700 cm^{-1} (−0.46 eV). [b] k_{SE} is the same regardless of the mediating state. [c] ω_1 = 1600 cm^{-1}; ω_2 = 50 cm^{-1}; log(k_{obs}) ≃ 0.26.

be increased and A decreased proportionally in eq 13 and the same answer will be obtained as long as $\sigma < 2\nu + 1$ (where $\nu = [\exp\{\hbar\omega/kT\} - 1]^{-1}$). Increasing the number of low-frequency modes increases the non-Condon effect for this particular configuration of potential surfaces, but this is not necessarily true for other configurations. As shown in Table V, the increase in rate constant tends to plateau for a large number of modes because the incremental change in Q_0 decreases as a single mode is divided into a larger number of modes. The magnitude of the non-Condon effect is affected by the value chosen for the damping Γ_{12} as shown in Figure 11. Typical values for Γ_{12} of tens of wavenumbers reduce the magnitude of the non-Condon effect by approximately 1 order of magnitude compared to Γ_{12} = 0.

A comparison of the non-Condon rate constants for various values of high- or low-frequency modes for both $P^+Q_A^-$ and $C_{H1}^+H^-$ as intermediate states is presented in Table VI. The differences in rate reflect the differences in Q_0 due to the configuration of the potential surfaces for each intermediate state.

TABLE VII: Non-Condon Calculation of the $C_{H2}^+Q_A^-$ Charge Recombination Rate Constant

$\lambda/\Delta G$[a]	log(k_{SE})[b]	$\Delta U(Q^*_{13})$, cm^{-1}	log(k_{NC})[c]	σ,[d] ×10^8	Q_0	A, ×10^{-7}
1.26	−13.3	775.0	−8.9	2.1	0.85	6.5
1.52	−11.8	649.0	−10.0	5.1	4.30	7.8
1.70	−13.0	2260.0	−9.0	6.3	0.79	23.0
1.96	−12.5	391.0	−12.5	3.7	7.9	4.0

[a] ΔG = 3200 cm^{-1} (−0.40 eV). [b] Calculated by using eq 11. [c] Mediating state, $C_{H1}^+Q_A^-$; a 50-cm^{-1} promoting mode was used in a two-mode calculatioin with a 1600-cm^{-1} mode; log(k_{exp}) ≃ −2.0. [d] Parameters used in eq 13.

A low-frequency mode (ω_2) gives a much larger enhancement of the rate constant for smaller values of the ratio $\lambda/\Delta G$ if $P^+Q_A^-$ is the intermediate state, and it has a maximum at $\lambda/\Delta G \simeq 1.7$ if $C_{H1}^+H^-$ is the intermediate state. If a high-frequency mode is used as the non-Condon coordinate, changes in rate constant appear more uniformly, ranging from a factor of 2 to 10 times larger at various values of $\lambda/\Delta G$.

The temperature dependence of the rate constant calculated including the non-Condon effect is quite mild. For the case of a high-frequency promoting mode, the temperature dependence with and without the Condon approximation is almost identical. For example, if λ = 5640 cm^{-1} (i.e., $\lambda/\Delta G$ = 1.52) the increase in rate constant between 100 and 200 K with and without the Condon approximation is 5% and 1%, respectively. For the case illustrated in Figure 10, when a low-frequency mode is the promoting mode, there is a 30% decrease in the non-Condon rate constant between 100 and 200 K, whereas the calculated rate constant by using either a high-frequency promoting mode or the Condon approximation decreases by 2% over this range in temperature. Similar results were found for other frequencies at all temperatures in the region below 200 K where an activationless rate was observed for $C_{H1}^+Q_A^-$ and $C_{H2}^+Q_A^-$ CR.[4,5]

4.3. Superexchange Including Non-Condon Effects for $C_{H2}^+Q_A^-$ Recombination. The calculated non-Condon effect for the $C_{H2}^+Q_A^-$ recombination reaction with a 50-cm^{-1} promoting mode and $C_{H1}^+Q_A^-$ intermediate is tabulated for four values of the reorganization energy in Table VII. The amplification factor A is larger and the standard deviation σ of the Gaussian is narrower for this reaction than for the $C_{H1}^+Q_A^-$ recombination reaction (compare Tables V and VII). The shapes of the free energy dependences are similar to those calculated for $C_{H1}^+Q_A^-$ (shown in Figure 10) and are not shown. Although significant enhancements in rate are found, the rate constants shown in Table VII are still smaller than the observed rate constant by many orders of magnitude.

4.4. Superexchange in $P^+Q_A^-$ and $P^+H_L^-$ Charge Recombination. Superexchange via $P^+H_L^-$ has been considered as a mechanism for the $P^+Q_A^-$ CR reaction in *Rb. sphaeroides* and has been found to be consistent with the experimentally determined FC factor.[10] In both *Rb. sphaeroides* and *Rps. viridis* the energy gap between $P^+Q_A^-$ and $P^+H_L^-$ is relatively large (Figure 2), so it is likely that the non-Condon effect is relatively small. Calculations confirm this, but it is also due to the fact that the reorganization energy for CR from the reactant and intermediate states ($P^+H_L^-$) is quite different (i.e., Q_0 is far from Q^*_{13} for the calculated configuration of potential energy surfaces, which are reasonable for $P^+Q_A^-$ CR).

The $P^+H_L^-$ recombination reaction may also occur by a superexchange mechanism via a bridge state such as $P^+B_L^-$. Although $P^+B_L^-$ has not been unambiguously observed, it has been considered as a possible intermediate for the initial CS reaction.[36-41] It is possible that a bridge state (whether real or virtual) that plays a role in the forward electron-transfer reaction would also participate in the electronic coupling of the recombination reaction for $P^+H_L^-$. If $P^+B_L^-$ is above the initially excited state ^1P in energy, the energy gap between this bridge state and

$P^+H_L^-$ is also large (>3000 cm^{-1} in *Rb. sphaeroides*).[88] The non-Condon effect is typically quite small for such a configuration of potential surfaces (i.e., a relatively large energy denominator ΔU). However, deep in the inverted region the deviation from the rate calculated by using the Condon approximation can still be significant as was shown in the model calculation in section 3 (see Figure 8).

4.5. Superexchange and the Primary Charge Separation Reaction. Although the estimated electronic coupling for the primary CS reaction, $^1P \rightarrow P^+H_L^-$, is quite small,[89] this reaction occurs in a few picoseconds. The electron-transfer matrix element between the states ^1P and $P^+H_L^-$ has been estimated from

$$J = \frac{V_{12}\Delta U_{22'}V_{2'3}}{\Delta U_{12}(Q^*_{21})\Delta U_{2'3}(Q^*_{2'3})} \qquad (18)$$

where J is the singlet–triplet splitting in the $P^+H_L^-$ radical pair state, V_{12} is coupling of the electron transfer ^1PH (state 1) $\rightarrow$ $P^+H_L^-$ (state 2), $V_{2'3}$ is the coupling between $P^+H_L^-$ (state 3) and ^3P (state 2'), and $\Delta U_{22'}$ is the singlet–triplet energy splitting between ^1P and ^3P. From the magnetic field effect on the ^3P quantum yield it is known that $J \simeq 10^{-3}$ cm^{-1}.[89] The ^3P decay rate as a function of temperature and magnetic field along with fluorescence and phosphorescence from ^3P gives $V_{22'} \simeq 3450$ cm^{-1}, $\Delta U_{21}(Q^*_{21}) \simeq 2100$ cm^{-1}, and $\Delta U_{2'3}(Q^*_{2'3}) \simeq 1450$ cm^{-1}.[90] By substitution of these values into eq 19 and under the assumption that V_{12} and $V_{2'3}$ are equal, $V_{12} \simeq V_{2'3} \simeq 1$ cm^{-1}. This coupling is too small to explain the initial electron-transfer rate constant if the rate constant is calculated within the Condon approximation (eq 6).

Several possibilities have been considered to resolve this dilemma.[41,91,92] An alternative to previous hypotheses is to relax the Condon approximation, because if the Condon approximation is not used, the relationship between the electronic coupling and the FC factor in eq 6 is no longer required to hold. Furthermore, a non-Condon effect is implied by a superexchange mechanism with a small energy gap between the reactant and intermediate states, and this is certainly the case if an intermediate state such as $P^+B_L^-$ is close in energy to ^1P.[36-41,78] Any calculation (e.g., that of ref 78) that assumes that the $P^+B_L^-$ intermediate state is close in energy to ^1PH_L must include the breakdown of the Condon approximation; however, this has not been previously considered. The motion along promoting modes in the state ^1PH can couple dimer charge-transfer states as well as interchromophore charge-transfer states, giving rise to a large non-Condon coupling. A relaxation of the $P^+H_L^-$ state has been proposed to explain observables such as the number of delayed fluorescence components on a variety of time scales, the magnetic field dependence of the fluorescence components, and the ^3P quantum yield in the large magnetic field (>150 kG) limit.[91,92] The model calculations for the recombination reactions (see above) show that it is possible for a relatively small relaxation of only 500 cm^{-1} to change the disposition of the nuclear potential energy surfaces, and thereby change the effective electronic coupling significantly. A more complete dynamical description of the coupling strength between exciton and charge-transfer states is required to determine if application of the non-Condon model presented above is appropriate for the primary CS reaction. One approach that we have persued in collaboration with Shreve et al. is resonance Raman of the electronic transition $P \rightarrow {}^1P$.[93] Those experiments suggest that some very low frequency dimer modes are strongly coupled to the electron-transfer reaction.[93] Further studies of the excitation profiles of low-frequency modes coupled to the transition $P \rightarrow {}^1P$ reveal whether there are any promoting modes in the manifold of ^1P (Shreve et al., to be published). Such experiments offer the possibility of obtaining specific information concerning the excited-state dynamics of ^1P and the role of strongly coupled intermediate states.

4.6. Superexchange and the Distance Dependence of Electron Transfer. Superexchange is bridge-mediated electron transfer and as such affects the distance dependence of electron-transfer reactions. The detailed experimental and theoretical studies of Gray, Onuchic, and Beratan and co-workers have shown that the through-bond and through-space pathways have a critical effect on the effective falloff α of the donor/acceptor coupling.[15,101] A similar conclusion was reached by Ulstrup and co-workers in studies of superexchange coupling in plastocyanin.[18] Likewise, the effect of bridge structure organic and inorganic donor/acceptor systems has been studied by many investigators[94] and the optimum geometry of transition-state complexes in fluid solution has been shown to depend more on the bridge geometry than on distance alone.[31] A superexchange model has been used by Miller and co-workers to explain long-distance electron-transfer in low-temperature glasses over distances of more than 30 Å.[72] The role of the solvent conduction band in low-temperature glasses has been considered by Albrecht[95] in systems where the tunneling distance of solvated electrons exceeds 50 Å. The considerations we have used to describe bridge states that possess an energy near that of the donor and acceptor are an extension of previous treatments of superexchange to include a bridge that is nearly resonant with the donor and acceptor while retaining a two-state calculation.

A recent article attempts to describe all electron-transfer reactions by using a single effective falloff of $\alpha = 1.4$ $Å^{-1}$.[96] As discussed in the Introduction, the concept of an exponential distance dependence has been discussed in the electron-transfer literature by a number of investigators.[31,50-52,72,94] In contrast to previous studies, the study by Moser et al.[96] interprets electron-transfer data obtained from RCs and semisynthetic Ru-modified hemoglobin in support of the conclusion that protein plays the role of a "uniform electronic barrier". The conclusion reached by Moser et al. is incompatible with superexchange as described by many investigators.[11-14,18,31,72] According to *any* superexchange model, the exponential falloff depends on the nature of the bridge (see, for example, refs 11–14, 18, 31, and 72 and the model calculation in section 3.3). Because the conclusion in ref 96 and the calculations outlined in this paper lead to such different pictures, in the following we discuss some of the relevant experimental data, both for the RC and model systems, that were not considered in ref 96.

It is clear from Figure 3 that the very long distance electron transfer reactions in *Rps. viridis* that are discussed at length in this paper are not compatible with a universal value of $\alpha \simeq 1.4$ $Å^{-1}$. In fact, only three out of the 11 observed electron-transfer reactions in *Rps. viridis* RCs conform to the "uniform electronic barrier" model. Moreover, at low temperature ($T < 200$ K) the model proposed by Moser et al.[96] fails for the RC. Both formation and recombination of $P^+Q_B^-$ are highly temperature dependent and the rate constant for both goes to zero below 200 K.[100] The cytochrome oxidation reaction ($P^+ \rightarrow C_{H1}^+$) is also highly temperature dependent, and the correlation that is adduced by Moser et al. does not hold for this process below 200 K.[61-65] Furthermore, at 295 K, citing the *same* reference used by Moser et al. for the $P^+ \rightarrow C_{H1}^+$ charge shift,[6] data are presented for $C_{H1}^+ \rightarrow C_{H2}^+$, which has a rate constant of 3×10^5 s^{-1} over a distance of 21 Å, and $P^+ \rightarrow C_{L1}^+$, which has a rate constant of 7×10^6 s^{-1} over a distance of 18 Å (at low redox potential), a discrepancy in both cases of more than 2 orders of magnitude from what is predicted by using $\alpha = 1.4$ $Å^{-1}$ (see also Table I). Moser et al. admit that the primary CS reaction obeys the uniform electronic barrier model only if the reaction is a two-step process and not if superexchange is the mechanism. The two-step mechanism has not been proven experimentally, and femtosecond transient absorption experiments as well as electric field effect experiments call the two-step proposal into question.[97-99]

The data discussed by Moser et al. for semisynthetic, protein-based systems do not follow the trend of a uniform electronic

barrier at long distance. Three of the six data points cited show no distance dependence at all with the same rate constant in ruthenated myoglobin for heme/His-81 Ru, heme/His-116 Ru, and heme/His-12 Ru at 19, 20, and 22 Å, respectively. The ruthenium at the His-48 position[101] (12.7-Å edge-to-edge distance) has a rate constant 2 orders of magnitude slower than that predicted by the uniform barrier model. In addition the rate constants of electron transfer in modified hemoglobins are more than 5 orders of magnitude slower than that predicted by the model.[102] More recent data suggesting a significant deviation from the exponential model are discussed by Gray and co-workers.[103] Moser and co-workers assert that proteins resemble amorphous glass solvents that have a uniform $\alpha = 1.2$ Å^{-1}, citing the work of Beitz and Miller.[104] In fact, Beitz and Miller do not indicate that there is a single exponential falloff for any given *solvent system* but rather that there is a given α for a given *donor*.[104] The reason for this is that the barrier height and, by extension, the probability amplitude of the donor wave function on the bridge depend on the energy difference between the donor and the bridge.[16] This idea has been tested systematically by Krongauz[105] who found values of α from 1.1 to 1.5, depending on the binding energy B of the donor (see section 2.2), although the effect of changing B is much weaker than predicted on the basis of a square barrier model. Gust and Moore and their co-workers have studied a series of synthetic compounds in which charge recombination has been examined for a fixed ultimate cation–anion pair.[106] The dimensions of these molecules is comparable to the RC, and, just as for the long-distance recombination reactions discussed here, long-distance recombinations in the model systems is found to have a much less steep distance dependence than would be predicted by a uniform barrier model. Just as for the RC, these model systems involve sequential charge separation steps, and the basic model of superexchange-mediated CR described throughout this paper is expected to apply. Similar results have been obtained in a related series of compounds prepared and Sessler and co-workers.[107]

In summary, we want to emphasize that superexchange is not an esoteric higher order effect, but rather it is a fundamental consideration that must be applied to any condensed-phase charge-transfer situation as has been discussed by many investigators. Superexchange as a model is equivalent to the statement that both the barrier height and tunneling distance are important for electron tunneling. The uniform electronic barrier model[96] is equivalent to the statement that only distance matters and the barrier height is irrelevant. According to the currently available literature, the latter model would appear to be unwarranted.

5. Conclusion

The exponential distance dependence that has been observed for charge-transfer reactions in a number of systems appears not to hold for electron transfer over long distances in photosynthetic reaction centers. This is likely due to the effect of mediating electronic states or superexchange. The cascade of CS reactions illustrated in Figure 2 results in a manifold of charge-transfer states that are close in energy. The cascade efficiently separates charge over long distances, but the manifold of states allows for recombination electron transfer over equally long distances. At room temperature recombination occurs via a thermal pathway for all of the charge-separated states (except perhaps the primary acceptor $P^+H_L^-$). The activated pathways have been elucidated and involve equilibria between each state and the higher-lying charge-transfer states, which act as real intermediates for activated recombination.[4,5,10] At low temperature these same electronic states can mediate the recombination reaction as virtual intermediates. Conventional superexchange as described in eq 11 improves the agreement between calculated and measured recombination rates in *Rps. viridis* considerably, and it has been shown that non-Condon effects can account for at least part of the remaining discrepancy.

While we have focused on what are probably the largest effects responsible for the electronic coupling in the long-distance electron transfer of the RC, there are a number of factors that may contribute to the rate constant that have not been considered. First, states of the protein may play a role in long-distance electronic coupling, and the coupling due to states described in this paper does not preclude the coupling pathways in the protein. Second, in considering a breakdown of the Condon approximation, we have only considered that contribution which is necessarily implied by eq 10 but not other contributions that may cause the individual matrix elements V_{12} or V_{23} to show non-Condon effects.

The model calculations presented here show that the assumption that the electronic factor is independent of the nuclear motion can lead to significant errors. Because it is difficult to calculate the electronic factor, treatments of electron-transfer rates typically take the separability of the electronic and nuclear factors for granted, and the electronic factor is used as an adjustable parameter. The long-standing problem of the temperature dependence of the cytochrome oxidation reaction suggests that electron-transfer theory which includes only the two principle redox centers (the donor and acceptor) may not account for important factors that govern the electron-transfer rate.

Acknowledgment. This paper is dedicated to Professor Harden McConnell, who first recognized the importance of superexchange in electron-transfer reactions,[12] on the occasion of his 65th birthday. We thank Drs. Andrew Shreve, Julian Joseph, and Kaiqin Lao for helpful discussions. This work was supported by a grant from the NSF Biophysics Program.

Appendix. Parameter Values for Calculating RC Electron-Transfer Rates

In order to calculate a non-Condon rate constant by using a superexchange model, the free energies, frequencies, electron-phonon coupling constants, and number of modes must be known in order to model the harmonic potential surfaces. The electronic couplings V_{12} and V_{23} must be known in order to determine the magnitude of the superexchange coupling.

A1. Free Energies. The internal energy of the reaction is the vertical difference between the minima of $U_1(Q)$, $U_2(Q)$, and $U_3(Q)$ (eq 7). In the absence of frequency shifts, the entropy change is zero and $-\Delta G = \Delta U$. Free energy values are taken from redox titrations,[88,4] activation parameters,[4] and delayed fluorescence measurements.[108] Values for the free energies obtained from equilibrium redox titrations do not necessarily apply to electron-transfer rates in the forward direction, as it is likely that relaxation (solvation) processes occur subsequent to these fast reactions. The free energy obtained from equilibrium redox titrations are likely to be more relevant for the slow CR reactions we are trying to model, because these occur subsequent to any relaxations about the charge-separated states.[109]

A2. Frequencies. The frequencies of modes coupled to $P^+Q_A^-$ CR are obtained from studies of either the electric field effect on kinetics[10] or quinone substitution experiments[110] in *Rb. sphaeroides* RCs. Those results are consistent with a total coupling ($S \simeq 2.5$) to an average high-frequency mode of $\sim$1600 cm^{-1} and a total coupling of $S \simeq 40$ to an average low-frequency mode between 50 and 200 cm^{-1}. In the absence of similarly detailed information for the cytochrome heme–quinone CR reactions, we will assume that the average frequencies of the modes coupled to those reactions are similar to those of $P^+Q_A^-$ recombination. This is reasonable since the main difference between these reactions is at the cationic site, which is a heme in $C_{H1}^+Q_A^-$ or $C_{H2}^+Q_A^-$ recombination and a bacteriochlorophyll dimer in $P^+Q_A^-$ recombination. Wraight and co-workers have shown that the temperature dependence of these reactions is

similar.[4] It is likely that the reorganization energy for the $C_{H1}^+Q_A^-$ and $C_{H2}^+Q_A^-$ CR reaction is larger than for $P^+Q_A^-$ CR, since the positive charge is more localized on a single heme than on a bacteriochlorophyll dimer. For the sake of comparison, the cytochrome heme–quinone CR reactions are studied by using four values of the ratio $\lambda/-\Delta G$.

A3. Electron–Phonon Couplings and the Number of Modes. In the Condon approximation, the electron–phonon couplings for modes of a given frequency are additive; i.e., 10 50-cm^{-1} modes with a coupling $S = 1.0$ are equivalent to one 50-cm^{-1} mode with a coupling $S = 10.0$. If non-Condon effects are included, however, the number of modes *does* matter, and the details of the shape of the nuclear potential surface are also become important. In the Results and Discussion section, the total electron–phonon coupling for high-frequency modes will be reported as S_1 and that for low-frequency modes S_2. However, if there are N low-frequency modes, the electron–phonon coupling constant for each mode is S_2/N; likewise for M high-frequency modes the linear coupling for each mode is S_1/M. The reorganization energy for M high-frequency and N low-frequency modes is

$$\lambda = \sum_{i=1}^{M}(S_1/M)\omega_1 + \sum_{j=1}^{N}(S_2/N)\omega_2 \qquad \text{(A1)}$$

The displacement of the intermediate state potential surface also changes with the number of modes, and this is included in the calculations.

Even with estimates for the frequencies and electron–phonon couplings in hand, it is very difficult to estimate the number of modes at a given frequency that are coupled to an electron-transfer reaction. A recent simulation of quantum dynamics of the charge-shift reaction $P^+H_L^- \rightarrow P^+Q_A^-$ in *Rb. sphaeroides*[111] gave estimates of the electron–phonon coupling on the order of $S \simeq 1.2$ for a 1600-cm^{-1} mode and $S \simeq 1.5$ for a 50-cm^{-1} mode. A calculation using crystal and EPR data gives $S \simeq 1.0$ for a 1600-cm^{-1} mode.[112]

A4. Electronic Coupling Matrix Elements. The electronic couplings estimated from the forward charge-shift reactions can be used to estimate the couplings for the CR reactions, which have been less well studied. The electronic matrix elements in Table I were calculated by using eq 6 and assuming that $\lambda \simeq -\Delta G$. This assumption may not be justified for the cytochrome heme oxidation reactions. The values of the electronic coupling used below are all based on the assumption of an electronic factor independent of the nuclear coordinate in the rate constant for the charge-shift reactions. Since the breakdown of the Condon approximation calls into question that independence, these values may require modification.

Despite an extensive literature[54] there is great uncertainty in the magnitude of the coupling between the cytochrome hemes and the special pair P. Assuming the C_{H1} and C_{H2} oxidation reactions are activationless ($\lambda \simeq -\Delta G$), a lower bound estimate for the electronic coupling of $V \simeq 0.2$ cm^{-1} and $V \simeq 0.07$ cm^{-1} is obtained for C_{H1} and C_{H2} oxidation, respectively. We use these values in the model calculations, although we recognize that they are lower bound estimates because if $\lambda \neq -\Delta G$ the FC term can only be smaller, implying that the electronic factor V^2 is larger (eq 6). The estimates for the electronic coupling of the $C_{L1}^+Q_A^-$ state to the $P^+Q_A^-$ state based on the assumption that $\lambda \gg -\Delta G$ have ranged from 2 to 20 cm^{-1}.[54] If the value of 2 cm^{-1} is applied to *Rps. viridis*, then the calculated rate constant for $C_{H1}^+Q_A^-$ CR from eq 11 would be larger by a factor of 10^2.

The charge-shift reactions that form the states $P^+Q_A^-$ and $C_{H1}^+Q_A^-$ do not involve intermediate redox states (see Figure 1). However, the C_{L1}, C_{H2}, and C_{L2} oxidation in the cytochrome may involve intermediate states. The extremely fast rate constant for the formation $C_{L1}^+Q_A^-$ suggests that the coupling of $C_{H1}^+Q_A^-$ to $C_{L1}^+Q_A^-$ is very strong and perhaps no longer in the nonadiabatic limit. The edge-to-edge distance from the vinyl group of C_{H1} to the heme macrocycle of C_{L1} is 4.5 Å. Similar distances are observed if the vinyl group is included in the edge-to-edge distance for C_{L1} to C_{H2} and C_{H2} to C_{L2}. This suggests that adjacent hemes are strongly coupled along the sequence C_{H1}–C_{L1}–C_{H2}–C_{L2} (see Figure 1).

The estimated coupling for the $C_{H1}^+C_{H2} \rightarrow C_{H1}C_{H2}^+$ charge shift is quite large considering the distance (Table I). It has been suggested that charge shift that forms the state $C_{H2}^+Q_A^-$ (at $E_m > 100$ mV) involves an intermediate state of the intervening redox center C_{L1}

$$C_{H2}C_{L1}{}^+C_{H1}{}^+Q_A^- \rightarrow C_{H2}{}^+C_{L1}C_{H1}{}^+Q_A^- \rightarrow C_{H2}{}^+C_{L1}{}^+C_{H1}Q_A^- \qquad \text{(A2)}$$

The energy gap between the C_{L1}^+ and the C_{H2} state is estimated to be 2400 cm^{-1} (0.30 eV) from the equilibrium redox potential of the respective hemes. According to a superexchange mechanism (eq 11) a coupling of $V_{12} \simeq V_{23} \simeq 10$ cm^{-1} between adjacent cytochrome hemes is consistent with the value, 0.07 cm^{-1} for C_{H2} oxidation in Table I. Although the rate constant is not known, C_{L1}^+ is oxidized by C_{L2} at cryogenic temperatures (if the redox potential is less than –80 mV), with a driving force of only 1000 cm^{-1}. Essentially the same intermediate state (virtual transfer from C_{L1}^+ to C_{H2}) is the lowest energy intermediate for C_{L2} oxidation by C_{L1}^+. Thus, the alternating low and high potential hemes can provide efficient coupling pathways under both reduced and oxidized conditions. A comparison of calculated through-protein pathways that includes superexchange via adjacent redox centers would provide an interesting test for the idea advanced here that superexchange via the redox centers is important and may help to explain the anomalous rates of the cytochrome heme oxidation reactions.[61-65]

In order to estimate the electronic matrix elements relevant to a superexchange calculation of the $P^+Q_A^-$ recombination reaction, values from *Rb. sphaeroides* are used because the $P^+H_L^-$ recombination reaction has not been studied in detail for *Rps. viridis* RCs. The reaction $P^+H_L^- \rightarrow P^+Q_A^-$ has an estimated coupling of $V \simeq 3.7$ cm^{-1}.[113] The magnitude of the electronic coupling for the $P^+H_L^-$ recombination reaction in *Rb. sphaeroides* has been estimated at $V \simeq 0.37$ cm^{-1}.[113] Due to the fact that this reaction is in the inverted region,[89] this is a lower bound. From these values, the electronic coupling for $P^+Q_A^-$ has been estimated to be ca. 3.0×10^{-4} cm^{-1} for *Rb. sphaeroides*.[10,113] According to eq 11, in *Rps. viridis* the $P^+Q_A^-$ reaction would have a larger coupling due to the fact that the energy of the $P^+H_L^-$ state is closer in energy to $P^+Q_A^-$ than in *Rb. sphaeroides*. Using the electronic coupling values of $V_{12} = 3.7$ cm^{-1} and $V_{23} = 0.37$ cm^{-1} from *Rb. sphaeroides* and the value of $\Delta U_{12} \simeq 2260$ cm^{-1} from *Rps. viridis*, we estimate the coupling for $P^+Q_A^-$ at 6.0×10^{-4} cm^{-1} in *Rps. viridis*. This value is consistent with the rate constant of 100 s^{-1} for the $P^+Q_A^-$ recombination reaction in *Rps. viridis*. Table III summarizes these estimates for the superexchange coupling of all states in the RC that may be relevant for the CR reactions.

References and Notes

(1) Deisenhofer, J.; Epp, O.; Miki, K.; Huber, R.; Michel, H. *J. Mol. Biol.* **1984**, *180*, 385–398.

(2) Allen, J. P.; Feher, G.; Yeates, T. O.; Komiya, H.; Rees, D. *Proc. Natl. Acad. Sci. U.S.A.* **1988**, *8*, 8487–8491.

(3) Chang, C.-H.; Tiede, D.; Tang, J.; Smith, U.; Norris, J.; Schiffer, M. *FEBS Lett.* **1986**, *205*, 82–86.

(4) Gao, J.; Shopes, R. J.; Wraight, C. A. *Biochim. Biophys. Acta* **1990**, *1015*, 96–108.

(5) Kaminskaya, O.; Konstantinov, A. A.; Shuvalov, V. A. *Biochim. Biophys. Acta* **1990**, *1016*, 153–164.

(6) Shopes, R. J.; Levine, L. M. A.; Holten, D.; Wraight, C. A. *Photosyn. React.* **1987**, *12*, 165–180.

(7) Shopes, R. J.; Wraight, C. A. *Biochim. Biophys. Acta* **1987**, *893*, 409–425.

(8) Kirmaier, C.; Holten, D. *Photosynth. Res.* **1987**, *13*, 225–260.

(9) Breton, J.; Martin, J.-L.; Migus, A.; Antonetti, A.; Orszag, A. *Proc. Natl. Acad. Sci. U.S.A.* **1986**, *83*, 5121–5125.

(10) Franzen, S.; Goldstein, R. F.; Boxer, S. G. *J. Phys. Chem.* **1990**, *94*, 5135–5149.
(11) Halpern, J.; Orgel, L. E. *Discuss. Faraday Soc.* **1960**, *29*, 32–41.
(12) McConnell, H. M. *J. Chem. Phys.* **1961**, *35*, 508–515.
(13) Onuchic, J. N.; Beratan, D. N. *J. Am. Chem. Soc.* **1987**, *109*, 6771–6777.
(14) Beratan, D. *J. Am. Chem. Soc.* **1986**, *108*, 4321–4326.
(15) Beratan, D. N.; Onuchic, J. N.; Hopfield, J. J. *J. Chem. Phys.* **1987**, *86*, 4488–4498.
(16) Freed, K. F. *J. Chem. Phys.* **1986**, *84*, 2108–2111.
(17) Beratan, D. N.; Hopfield, J. J. *J. Chem. Phys.* **1984**, *81*, 5753–5759.
(18) Christensen, H. E. M.; Conrad, L. S.; Mikkelsen, K. V.; Nielsen, M. K.; Ulstrup, J. *Inorg. Chem.* **1990**, *29*, 2808–2816.
(19) Mikkelsen, K. V.; Ulstrup, J.; Zakaraya, M. G. *J. Am. Chem. Soc.* **1989**, *111*, 1315–1319.
(20) Kuznetsov, A. M.; Ulstrup, J. *Phys. Stat. Sol. (b)* **1982**, *114*, 673–683.
(21) Kim, H. J.; Hynes, J. T. *J. Phys. Chem.* **1990**, *94*, 2736–2740.
(22) Gutsche, E. *Phys. Stat. Sol.* **1982**, *109*, 583–597.
(23) Nitzan, A.; Jortner, J. *J. Chem. Phys.* **1972**, *56*, 3360–3373.
(24) Fujimura, Y.; Kono, H.; Nakajima, T. *J. Chem. Phys.* **1976**, *66*, 199–206.
(25) Freed, K.; Lin, S. H. *Chem. Phys.* **1975**, *11*, 409–432.
(26) Spears, K. G.; Rice, S. A. *J. Chem. Phys.* **1971**, *55*, 5561–5581.
(27) Suzuki, T.; Ito, M. *J. Chem. Phys.* **1989**, *91*, 4564–4570.
(28) Hornburger, H. *Z. Phys. D: At., Mol. Cluster* **1989**, *11*, 129–139.
(29) Sobolewski, A. L. *Chem. Phys.* **1987**, *115*, 469–479.
(30) Penner, A. P.; Siebrand, W.; Zgierski, M. Z. *J. Chem. Phys.* **1978**, *69*, 5496–5508.
(31) Newton, M. D. *Chem. Rev.* **1991**, *91*, 767–792.
(32) Lin, S. H. Personal communication.
(33) Joseph, J. S. Ph.D. Thesis, University of California at Berkeley.
(34) Reimers, J. R.; Hush, N. S. *Chem. Phys.* **1988**, *134*, 323–354.
(35) Rendell, A. P. L.; Bacskay, G. B.; Hush, N. S. *J. Am. Chem. Soc.* **1988**, *110*, 8343–8354.
(36) Hu, Y.; Mukamel, S. *Chem. Phys. Lett.* **1989**, *160*, 410–416.
(37) Bixon, M.; Jortner, J. *Photosyn. Res.* **1989**, *22*, 29–37.
(38) Scherer, P. O. J.; Fischer, S. F. *Chem. Phys. Lett.* **1986**, *131*, 153–159.
(39) Plato, M.; Mobius, K.; Nichel-Beyerle, M. E.; Bixon, M.; Jortner, J. *J. Am. Chem. Soc.* **1988**, *110*, 7279–7285.
(40) Warshel, A.; Creighton, S.; Parson, W. W. *J. Phys. Chem.* **1988**, *92*, 2696–2701.
(41) Won, Y.; Friesner, R. A. *Biochim. Biophys. Acta* **1988**, *935*, 9–18.
(42) Goldstein, R. F.; Franzen, S. F.; Bialek, W., submitted.
(43) Alegria, G.; Dutton, P. L. *Biochim. Biophys. Acta* **1991**, *1057*, 258–272.
(44) Vermeglio, A.; Richaud, P.; Breton, J. *FEBS Lett.* **1989**, *243*, 259–263.
(45) Nitschke, W.; Rutherford, W. A. *Biochemistry* **1989**, *28*, 3161–3168.
(46) Hubbard, J. A. M.; Evans, M. C. W. *FEBS Lett.* **1989**, *244*, 71–75.
(47) Dracheva, S. M.; Drachev, L. A.; Konstantinov, A. A.; Semenov, A. Y.; Skulachev, V. P.; Arutjunjan, A. M.; Shuvalov, V. A.; Zaberezhnaya, S. M. *Eur. J. Biochem.* **1988**, *171*, 253–264.
(48) A recent study by Shuvalov and co-workers[5] confirms the kinetic scheme in ref 4; however, at 77 K, the $C_{H1}^{+}Q_A^{-}$ CR reaction was found to be an order of magnitude faster and the $C_{H2}^{+}Q_A^{-}$ approximately 1 order of magnitude slower than those reported by Gao et al.[4] The $C_{H1}^{+}Q_A^{-}$ CR rate constant depends on the duration of the excitation flash (Shuvalov, V., personal communication). The key observation that suggests nuclear tunneling is the temperature-independent electron transfer below 240 K reported in ref 4 and corroborated by 77 K experiments in ref 5.
(49) There is strong similarity between the cytochrome oxidation reactions in *C. vinosum* and *Rps. viridis*, which has been discussed in detail in the literature (e.g., ref 60). It is interesting that the recombination reaction of $C_{L1}^{+}Q_A^{-}$ in *C. vinosum* appears to be a factor of 10^4 slower than that from C_{H1} (at room temperature).[63] At low temperature in *C. vinosum* the C_{L1} oxidation reaction is irreversible. In *Rps. viridis* it is extremely slow if not irreversible.[64] The nuclear factor may also play a role in the temperature dependence of the $C_{L1}^{+}Q_A^{-}$ CR reaction. The driving force of this CR is about 800 cm^{-1} and the reorganization energy is likely about 4000 cm^{-1} or more. These considerations apply to many other species of RC.[65]
(50) Zamaraev, K. I.; Khairutdinov, R. F.; Miller, J. R. *Chem. Phys. Lett.* **1978**, *57*, 311–315.
(51) Hush, N. S. *Coord. Chem. Rev.* **1985**, *64*, 135–157.
(52) Wasielewski, M. In *Photoinduced Electron Transfer, Part A*; Fox, M. A., Chanon, M., Eds.; Elsevier Science Publishing Co.: New York, 1988; pp 161–227.
(53) The distance between redox centers is often corrected for the van der Waals radii, thus reducing the value of R by ca. 3.5 Å. This has not been done here as we are concerned with trends at very long distances and such a correction, if needed, does not affect the conclusions in this paper. The calculation of ET rates using this formalism is valid only for nonadiabatic electron-transfer reactions.
(54) DeVault, D. *Quantum-Mechanical Tunneling in Biological Systems*; Cambridge University Press: Cambridge, 1984.
(55) Ulstrup, J.; Jortner, J. *J. Chem. Phys.* **1975**, *63*, 4358–4368.
(56) Johnson, M. D.; Miller, J. R.; Green, N. S.; Closs, G. L. *J. Phys. Chem.* **1989**, *23*, 1173–1176.
(57) The distance dependence of the reorganization energy due to modes for which $\hbar\omega \ll kT$ is part of the nuclear factor and has been discussed.[58] This effect can be large if the outer-sphere reorganization energy is large.
(58) Isied, S. S.; Vassilian, A.; Wishart, J. F.; Creutz, C. C.; Schwartz, H. A.; Sutin, N. *J. Am. Chem. Soc.* **1988**, *110*, 635–637.
(59) The rate of $P^{+}H_L^{-}$ recombination reaction in *Rps. viridis* is similar to that observed in *Rb. sphaeroides*.[60] The energy gap between the state $P^{+}H_L^{-}$ and the ground state is 0.9 eV in *Rps. viridis*. Due to the mild temperature dependence of the primary CS it is often assumed that $\lambda \simeq -\Delta G$ for this reaction (i.e., $\lambda < 0.4$ eV). The reorganization energy for the CR reaction is likely to be similar, thus, for $P^{+}H_L^{-}$ CR, $\Delta G > \lambda$.
(60) Holten, D.; Windsor, M. W.; Parson, W. W.; Thornber, J. P. *Biochim. Biophys. Acta* **1978**, *501*, 112–126.
(61) DeVault, D.; Chance, B. *Biophys. J.* **1966**, *6*, 825–847.
(62) Case, G. D.; Parson, W. W.; Thornber, J. P. *Biochim. Biophys. Acta* **1970**, *223*, 122–128.
(63) Siebert, M.; DeVault, D. *Biochim. Biophys. Acta* **1971**, *253*, 396–411.
(64) Kihara, T.; Chance, B. *Biochim. Biophys. Acta* **1969**, *189*, 116–124.
(65) Kihara, T.; Dutton, P. L. *Biochim. Biophys. Acta* **1970**, *205*, 196–204.
(66) Landau, L. D.; Lifschitz, E. M. *Quantum Mechanics*; Pergamon Press: Oxford, 1974.
(67) Fischer, G. *Vibronic Coupling*; Academic Press: London, 1984.
(68) Teichler, H. *Phys. Stat. Sol. (b)* **1981**, *104*, 239–250.
(69) The zero of the coordinate system in this description is at the reactant's minimum. In the calculation of the promoting mode correlation function, the zero is located halfway between the reactant's and product's minima. Thus $\eta_i/2$ must be subtracted from any parameters calculated that depend on position with respect to the ith nuclear coordinate.
(70) The dephasing rate $1/T_2 = 1/2T_1 + 1/T_2^{*}$ contains contributions from the population relaxation rate out of the state, $1/2T_1$, as well as the pure dephasing rate, $1/T_2^{*}$.
(71) There is a nuclear coordinate dependence implicit in an exponential distance dependence (such as in eq 2) and any normal mode with components that change the distance between the donor and acceptor will be promoting modes. However, given the small extent of typical root-mean-square displacements and the known exponential functional form, this effect is likely to be small. The calculation of a non-Condon effect with an exponential dependence on the nuclear coordinate is discussed elsewhere.[42]
(72) Miller, J. R.; Beitz, J. V. *J. Chem. Phys.* **1981**, *74*, 6746–6756.
(73) Kosloff, R.; Ratner, M. *Isr. J. Chem.* **1990**, *30*, 45–58.
(74) We have used the magnitude of eq 10 for the analysis presented here. The magnitude of the coupling due to the real part of eq 10 is zero on-resonance and depends on the magnitude of the detuning energy and dephasing Γ_{12} or Γ_{23} off-resonance (i.e., when ΔU_{12} or $\Delta U_{23} \neq 0$). The imaginary part is never zero unless $\Gamma_{12} = 0$ or $\Gamma_{23} = 0$ and decreases in magnitude as either ΔU_{ij}, Γ_{12}, or Γ_{23} is increased.
(75) This exposition includes the failure of the Condon approximation only at the level of the coordinate dependence of the perturbative coupling of a single intermediate state. The cumulative effect of a cascade of CS reactions such as that shown in Figure 2 has not been included and is likely to further enhance the recombination rates.
(76) The electronic coupling given in eq 10 must be squared in order to calculate the non-Condon matrix element (eq 16 in ref 42). Since the square of the Gaussian term that results has poles, it is not appropriate to evaluate the constant term and cross term in the same integral. The saddle point and integration contour for the cross term are difficult to compute for more than one mode (even if there is only one promoting mode). However, the cross term will always be negligible as long as $A(2\pi)^{1/2}\sigma \not\ll 1$ in eq 13 (i.e., the Gaussian and constant terms are not equal in magnitude). Depending on the configuration of the potential surfaces, either the constant or Gaussian term dominates, and therefore the cross term has been neglected.
(77) Levich, V. G.; Dogonadze, R. R. *Dokl. Akad. Nauk SSSR* **1959**, *124*, 123–126.
(78) Bixon, M.; Jortner, J. J.; Michel-Beyerle, M. E. *Biochim. Biophys. Acta* **1990**, *1056*, 301–315.
(79) Metz, F. *Chem. Phys.* **1975**, *9*, 121–134.
(80) Berg, M.; Walsh, C. A.; Narasimhan, L. R.; Littau, K. A.; Fayer, M. D. *Chem. Phys. Lett.* **1987**, *139*, 66–71.
(81) Middendorf, T. R.; Mazzola, L. M.; Gaul, D. F.; Schenck, C. C.; Boxer, S. G. *J. Phys. Chem.* **1991**, *95*, 10142–10151.
(82) Johnson, S. G.; Tang, D.; Jankowiak, R.; Hayes, J. M.; Small, G. J.; Tiede, D. M. *J. Phys. Chem.* **1990**, *94*, 5849–5855.
(83) Myers, A. B.; Mathies, R. A. In *Biological Applications of Raman Spectroscopy*; Spiro, T. G., Ed.; John Wiley & Sons: New York, 1987; Vol. 2, Resonance Raman Spectra of Polyenes and Aromatics, pp 1–57.
(84) Schomaker, K. T.; Champion, P. M. *J. Chem. Phys.* **1989**, *90*, 5982–5993.
(85) Robert, B.; Lutz, M. *Biochemistry* **1986**, *25*, 2304–2309.
(86) Hashimoto, H.; Koyama, Y. *Biochim. Biophys. Acta* **1990**, *1017*, 181–186.
(87) All of the processes considered thus far involve one-electron exchange processes between the redox centers. A one-electron integral that couples C_{H1}^{+} to C_{H2}^{+} via C_{L1}^{+} requires the coupling between the high-potential cytochrome hemes and C_{L1} to be greater than 10 cm^{-1}. As discussed in the Appendix such a value is plausible; however, because the superexchange coupling obtained by using such a value is approximately equal to 0.08 cm^{-1}, which is the same as the value calculated in Table I, the $C_{H2}^{+}Q_A^{-}$ recombination

rate constant is not significantly changed. A two-electron exchange involving simultaneous virtual hole transfer from $C_{L1}^+ \rightarrow C_{H1}$ and $C_{H2}^+ \rightarrow C_{L1}$ could play a role in $C_{H2}^+Q_A^-$ CR.

(88) Prince, R. C.; Leigh, J. S.; Dutton, P. L. *Biochim. Biophys. Acta* **1976**, *440*, 622–636.

(89) Marcus, R. A. *Chem. Phys. Lett.* **1987**, *133*, 471–477.

(90) Goldstein, R. A.; Takiff, L. T.; Boxer, S. G. *Biochim. Biophys. Acta* **1988**, *934*, 153–163.

(91) Woodbury, N. W.; Parson, W. W. *Biochim. Biophys. Acta* **1984**, *767*, 345–361.

(92) Goldstein, R. A.; Boxer, S. G. *Biochim. Biophys. Acta* **1989**, *977*, 78–86.

(93) Shreve, A. P.; Cherepy, N. J.; Franzen, S.; Boxer, S. G.; Mathies, R. A. *Proc. Natl. Acad. Sci. U.S.A.* **1991**, *88*, 11207–11211.

(94) Siddarth, P.; Marcus, R. A. *J. Phys. Chem.* **1990**, *94*, 2985–2989.

(95) Doheny, A. J.; Albrecht, A. C. *Can. J. Chem.* **1977**, *55*, 2065–2079.

(96) Moser, C. C.; Keske, J. M.; Warncke, K.; Farid, R. S.; Dutton, P. L. *Nature* **1992**, *355*, 796–802.

(97) Lockhart, D. J.; Hammes, S. L.; Franzen, S.; Boxer, S. G. *J. Phys. Chem.* **1991**, *95*, 2217–2226.

(98) Eberl, U.; Ogrodnik, A.; Michel-Beyerle, M. E. *Z. Naturforsch.* **1990**, *45a*, 763–770.

(99) Breton, J.; Martin, J.-L.; Migus, A.; Antonetti, A. *Proc. Natl. Acad. Sci. U.S.A.* **1986**, *83*, 5121–5125.

(100) Kleinfeld, D.; Okamura, M. Y.; Feher, G. *Biochemistry* **1984**, *23*, 5780–5786.

(101) Gray, H. B.; Malmström, B. G. *Biochemistry* **1989**, *28*, 7499–7505.

(102) Kuila, D. W.; Baxter, W.; Natan, M. J.; Hoffman, B. M. *J. Phys. Chem.* **1991**, *95*, 1–3.

(103) Onuchic, J. N.; Beratan, D. N.; Winkler, J. R.; Gray, H. *Annu. Rev. Biophys. Biomol. Struct.* **1992**, *21*, 349–377.

(104) Miller, J. R.; Beitz, J. V.; Huddleston, R. K. *J. Am. Chem. Soc.* **1984**, *106*, 5057–5068.

(105) Krongauz, V. V. *J. Phys. Chem.* **1992**, *96*, 2609–2613.

(106) Gust, D.; Moore, T. A.; Moore, A. L.; Lee, S.-J.; Bittersmann, E.; Luttrull, D. K.; Rehms, A. A.; DeGraziano, J. M.; Ma, X. C.; Gao, F.; Belford, R. E.; Trier, T. T. *Science* **1990**, *248*, 199–201.

(107) Rodriguez, J.; Kirmaier, C.; Johnson, M. R.; Friesner, R. A.; Holten, D.; Sessler, J. L. *J. Am. Chem. Soc.* **1991**, *113*, 1652.

(108) Arata, H.; Parson, W. W. *Biochim. Biophys. Acta* **1981**, *638*, 201–209.

(109) The free energy used for the calculation of non-Condon effects was based on the value of 0.52 eV for $P^+Q_A^-$ recombination in *Rb. sphaeroides*. This is 0.1 eV lower than the value in *Rps. viridis*. We used this value because our estimate of the reorganization energy derives from electric field effect work done on *Rb. sphaeroides*.[10]

(110) Gunner, M. R.; Robertson, D. E.; Dutton, P. L. *J. Phys. Chem.* **1986**, *90*, 3783–3794.

(111) Warshel, A.; Chu, Z. T.; Parson, W. W. *Science* **1989**, *246*, 112–116.

(112) Onuchic, J. N.; Goldstein, R. F.; Bialek, W. In *Perspectives in Photosynthesis*; Proc. of the 22nd Jerusalem Symposium on Quantum Chem. and Biochem.; Jortner, J., Pullman, B., Eds.; Reidel Publishing Co.: Dordrecht, 1989.

(113) Bixon, M.; Jortner, J. *J. Phys. Chem.* **1986**, *90*, 3795–3800.